New H₂O masers in Seyfert and FIR bright galaxies

IV. Interferometric follow-ups[⋆]

A. Tarchi[1], P. Castangia[1], C. Henkel[2], G. Surcis[3,⋆⋆], and K. M. Menten[2]

[1] INAF-Osservatorio Astronomico di Cagliari, Loc. Poggio dei Pini, Strada 54, 09012 Capoterra (CA), Italy
e-mail: atarchi@oa-cagliari.inaf.it
[2] Max-Planck-Insitut für Radioastronomie, Auf dem Hügel 69, 53121 Bonn, Germany
[3] Argelander-Institut für Astronomie der Universität Bonn, Auf dem Hügel 71, 53121 Bonn, Germany

Received 1 April 2010 / Accepted 23 August 2010

ABSTRACT

Context. Very luminous extragalactic water masers, the megamasers, are associated with active galactic nuclei (AGN) in galaxies characterized by accretion disks, radio jets, and nuclear outflows. Weaker masers, the kilomasers, seem to be related mostly to star formation activity, although the possibility exists that some of these sources may belong to the weak tail of the AGN maser distribution.
Aims. It is particularly important to accurately locate the water maser emission to reveal its origin and shed light on extragalactic star-forming activity or to elucidate the highly obscured central regions of galaxies.
Methods. We performed interferometric observations of three galaxies, NGC 3556, Arp 299, and NGC 4151, where water emission was found. Statistical tools were used to study the relation between OH and H₂O maser emission in galaxies.
Results. The maser in NGC 3556 is associated with a compact radio continuum source that is most likely a supernova remnant or radio supernova. In Arp 299, the luminous water maser has been decomposed in three main emitting regions associated with the nuclear regions of the two main galaxies of the system, NGC 3690 and IC 694, and the region of overlap. In NGC 4151, only one of the two previously observed maser components has been tentatively detected. This feature, if real, is associated with the galaxy's central region. The only galaxy, so far, where luminous maser emission from two maser species, OH and H₂O, has been confidently detected is Arp 299. Weaker masers from these two species instead coexist in a number of objects. A search for emission from both maser species in a larger number of galaxies is, however, needed to assess these last two results better.

Key words. masers – galaxies: active – galaxies: nuclei – galaxies: starburst – radio lines: galaxies

1. Introduction

While there is unanimous consent that the most luminous H₂O masers are related to the nuclear activity of their host galaxies (accretion disks, nuclear jets, or outflows), the origins of the weaker extragalactic masers, i.e. the "kilomasers", are still a matter of debate. Unlike the megamasers, the observed luminosities ($L_{H_2O} < 10 L_\odot$) of kilomasers can be explained by the superposition of several galactic W49N-like or even weaker sources. Furthermore, most of the known kilomasers are associated with particularly active star-forming regions clearly offset from the nucleus of their parent galaxy (e.g., M 33, Churchwell et al. 1977). This has led to the belief that kilomasers and megamasers may constitute two distinct classes of extragalactic H₂O masers. Most of the former are related to star formation similar to, although typically brighter than, the galactic masers, while the latter are thought to be exclusively powered by the nuclear activity of active galactic nuclei (AGN). The kilomaser sources associated with the active galactic nuclei of M 51 (Hagiwara et al. 2001b) and of a few more H₂O masers of lower luminosity in the inner parsecs of NGC 4051 (Hagiwara et al. 2003), NGC 520 (Castangia et al. 2008), and NGC 3620 (Surcis et al. 2009)

hint at the possibility that some kilomasers could also be related to nuclear activity, providing the low-luminosity tail of the more powerful megamasers.

To date, beyond the Magellanic Clouds, the presence of 32 kilomasers has been reported from 24 galaxies (see Table 3). The maser emission from 16 of these galaxies has not yet been studied at high resolution so that it is impossible to draw definite conclusions on its nature. This and the impact such measurements have on pinpointing spots of vigorous star formation or elucidating properties of nearby AGN has motivated extended searches for more such masers, as well as interferometric follow-ups, to determine their origin.

With this goal in mind, we performed Very Large Array (VLA[1]) observations of the kilomaser source NGC 3556, detected in our far infrared (FIR) sample comprised of all galaxies with IRAS Point Source 100 μm flux density >50 Jy and Dec. > −30° (Henkel et al. 2005, hereafter HPT). In addition, we used the VLA to observe the megamaser in Arp 299, which is part of the same sample, and it appears to arise from more than one spot (Tarchi et al. 2007b). Finally, we also present interferometric data from NGC 4151, a Seyfert galaxy hosting a kilomaser with unusual features.

---

[1] The National Radio Astronomy Observatory (NRAO) is operated by Associated Universities, Inc., under a cooperative agreement with the National Science Foundation.

In Sects. 2 and 3, we describe the observations and results, respectively. Section 4 associates the detected masers with either star formation or AGN activity and analyses statistically the extragalactic H_2O and OH (kilo)masers known to date. Main conclusions are summarized in Sect. 5. The present work is the last in a series of papers (Henkel et al. 2005; Castangia et al. 2008; Surcis et al. 2009) that report searches for water maser emission in complete FIR-flux based samples of galaxies, highlight new water maser line detections, and present detailed maps of their surroundings.

2. Observations

All galaxies were observed in spectral line mode, in the $6_{16} \rightarrow 5_{23}$ transition of ortho-H_2O (rest frequency 22.23508 GHz).

2.1. NGC 3556

NGC 3556 was observed with the VLA in two hybrid configurations, CnB on September 28, 2002 and DnA on January 25, 2006. In both cases, observations were made by employing a single band of width 6.25 MHz centered on the velocity of the maser feature detected with Effelsberg (740 km s^{-1}; HPT). The observing band was subdivided into 128 channels each of width 48.8 kHz, which corresponds to ~0.7 km s^{-1}. The flux density scale was determined in both observing runs by measuring the nonvariable source 3C 286, with an adopted flux density of 2.54 Jy, as calculated by the NRAO's Astronomical Image Processing System (AIPS) task SETJY using the revised (by Perley) scale of Baars et al. (1977). The phase calibrator was 11282+59252, whose flux density was estimated to be 0.56 ± 0.01 Jy and 0.65 ± 0.01 Jy in the two runs, respectively. We also used 3C 286 to determine the bandpass corrections. On January 5, 2008, NGC 3556 was also observed at 1.4 GHz by the Multi-Element Radio Linked Interferometer Network (MERLIN[2]) in wide-field continuum mode for a total on-source integration time of 18 h. The sources 3C 286 and 1055+567 were used as flux and phase calibrators, respectively.

2.2. Arp 299

Water vapor in Arp 299 was observed on September 19, 2004 and April 9, 2007 with the VLA in its A and D configurations, respectively. A frequency setup with two 25 MHz intermediate frequency bands ("IFs") centered on local standard of rest velocities of V_{LSR} = 2900 and 3200 km s^{-1} was used. The IFs were overlapped in frequency to minimize the effect of band-edge roll-off. Each IF covered ~340 km s^{-1} with a resolution of ~20 km s^{-1}. For both datasets, the flux density and bandpass calibration was performed by using 3C 286 (2.56 Jy) and the phase calibration was derived from observations of the point source 11282+59252 (0.53 ± 0.01 for the A and 0.30 ± 0.01 Jy for the D array, respectively). Radio continuum maps were produced using the (few) line-free channels. For the A-array data, the restoring beam was $0\rlap{.}{''}1 \times 0\rlap{.}{''}1$, and the rms noise was 0.5 mJy/beam/chan and 0.25 mJy/beam for the cube and the continuum maps, respectively. The noise was higher than the expected thermal noise, likely because of poor weather during the observations. For the D-array data, the restoring beam was $4\rlap{.}{''}9 \times 4\rlap{.}{''}0$ and the rms noise was 0.25 mJy/beam/chan and 0.1 mJy/beam for individual spectral channels and the continuum maps, respectively. Spectral line

22-GHz single-dish observations of the water maser in Arp 299 were also performed with the 100-m Effelsberg radio telescope in November 2005 by pointing at the three main centers of activity in the system (see Sect. 3.2) and in April 5, 2007 (only four days before the VLA D-array measurements) with a single pointing midway between the three aforementioned locations.

2.3. NGC 4151

NGC 4151 was observed with the VLA in its DnA hybrid configuration on January 25, 2006. Observations were made using two 3.125-MHz IFs centered at the velocity of the two maser features detected with the GBT (692 and 1127 km s^{-1}, respectively; Braatz et al. 2004). Each IF was subdivided into 128 channels that provide a channel spacing of 24.4 kHz corresponding to ~0.33 km s^{-1}. The flux density scale and bandpass corrections were determined by using 3C 286 (2.54 Jy). The phase calibration was derived from observations of 11470+39586 (0.88 ± 0.01 Jy).

2.4. Data reduction and position accuracy

The data reduction was made using AIPS. All datasets were calibrated in the standard way. The radio continuum emission was subtracted from the spectral line data using AIPS task UVLSF, which fits a straight line to the visibilities of the line-free channels and then subtracts it from the uv dataset. This task also provides the fitted baseline as an uv dataset that was used to create continuum maps. Each individual dataset was Fourier-transformed using natural weighting and then deconvolved utilizing the CLEAN algorithm (Högbom 1974). Details of the observations and of the interferometric maps are summarized in Table 1.

The accuracy on absolute positions in a map due to statistical errors can be estimated using the synthesized beam size divided by the signal-to-noise ratios. For details on this derivation see, e.g., Hagiwara et al. (2001a). For our observations taken in the VLA D and CnB-array configurations, given their relatively coarse resolution, the statistical errors dominate, so they are representative of the positional accuracy for the maps produced. For the VLA A and DnA-array maps, the positional uncertainties are dominated by the error due to the different position of the phase calibrator w.r.t. that of the target galaxies. The nominally estimated error for absolute positions in this case is $0\rlap{.}{''}1$. Since in our measurements we used the "fast switching" technique and since errors can be divided by the signal-to-noise ratio (see above), this value can be taken as a safe upper limit (see, e.g., Tarchi et al. 2007a). Coordinates of the maser peaks in our VLA maps and associated positional errors are reported in Table 2.

The relative positions between line and continuum peak positions derived from the same data is only limited by the signal-to-noise ratios since the uncertainty caused by the different position of the calibrator w.r.t. that of the target galaxy affects both positions in the same way and cancels out. As a result, for our data we estimate the error on relative positions to be $\sigma_{rel} = \sqrt{(\theta_l/(2 \cdot SNR_l))^2 + (\theta_c/(2 \cdot SNR_c))^2}$, where θ denotes the restored beam size of the map in use, and l and c refer to line and continuum emission (for details, see also Tarchi et al. 2007a, and references therein). When the line and peak positions are instead derived by different datasets, the final accuracy can be estimated by the quadratic sum of the errors on the absolute positions in the two maps.

---

[2] MERLIN is a National Facility operated by the University of Manchester at Jodrell Bank Observatory on behalf of STFC.

Table 1. Interferometric maps.

Source	Epoch	Telescope	Mode	Freq. (GHz)	Bandwidth (MHz)	IFs No.	Channel width (kHz)	Weighting	Beam size	rms (mJy beam^{-1} chan^{-1})
NGC 3556	28-Sep.-02	VLA-CnB	Line	22	6.25	1	48.8	Natural	$1\rlap{.}''15 \times 0\rlap{.}''43$	4
NGC 3556	25-Jan.-06	VLA-DnA	Line	22	6.25	1	48.8	Natural	$0\rlap{.}''27 \times 0\rlap{.}''19$	3.5
NGC 3556	5-Jan.-08	MERLIN	Cont.	1.4	16	1	–	Natural	$0\rlap{.}''22 \times 0\rlap{.}''17$	0.04
NGC 3556	5-Jan.-08	MERLIN	Cont.	1.4	16	1	–	Uniform	$0\rlap{.}''16 \times 0\rlap{.}''14$	0.05
Arp 299	19-Sep.-04	VLA-A	Line	22	16.0	2	1562.5	Natural	$0\rlap{.}''10 \times 0\rlap{.}''10$	0.5
Arp 299	9-Apr.-07	VLA-D	Line	22	16.0	2	1562.5	Natural	$4\rlap{.}''89 \times 4\rlap{.}''03$	0.25
NGC 4151	25-Jan.-06	VLA-DnA	Line	22	3.125	2	24.4	Natural	$0\rlap{.}''24 \times 0\rlap{.}''11$	10

Table 2. Parameters of the maser lines observed with the VLA.

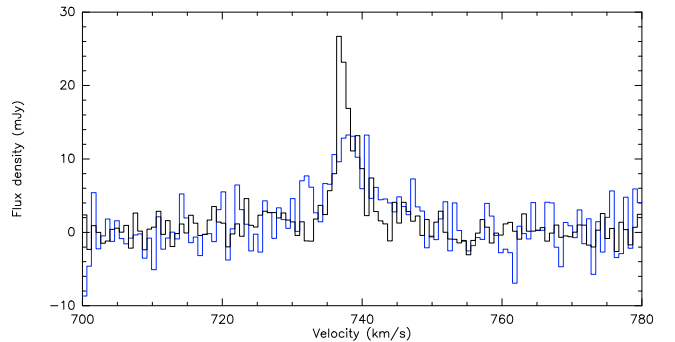| Source	Distance (Mpc)	Array	Peak coordinates[a] RA	Dec.	$V_{\rm LSR,opt}$[b] (km s^{-1})	$\int S\,dV$[b] (Jy km s^{-1})	$L_{\rm H_2O}$[c] ($L_\odot$)	Notes
NGC 3556	12	CnB	11 11 31.46 ± 0.02	+55 40 28.8 ± 0.2	738.2 ± 0.7	0.087 ± 0.004	0.29 ± 0.01	
NGC 3556	12	DnA	11 11 31.47 ± 0.01	+55 40 28.7 ± 0.1	737.5 ± 0.1	0.083 ± 0.005	0.28 ± 0.01	
Arp 299								
– IC 694	42	A	11 28 33.65 ± 0.01	+58 33 46.8 ± 0.1	2996 ± 8	0.16 ± 0.03	6.4 ± 1.2	
		D	11 28 33.65 ± 0.01	+58 33 46.8 ± 0.1	2988 ± 2	0.46 ± 0.03	19 ± 1	
– NGC 3690	"	A	11 28 30.99 ± 0.01	+58 33 40.7 ± 0.1	3112 ± 8	0.41 ± 0.05	17 ± 2	
		D	11 28 30.97 ± 0.02	+58 33 40.8 ± 0.2	3112 ± 4	0.55 ± 0.03	22 ± 1	
– C+C'-complex	"	A	11 28 30.63 ± 0.01	+58 33 52.4 ± 0.1	3179 ± 18	0.18 ± 0.04	7.5 ± 1.5	tentative
C'		D	11 28 31.35 ± 0.02	+58 33 49.8 ± 0.2	3158 ± 4	0.30 ± 0.04	12 ± 2	
C		D	11 28 30.65 ± 0.11	+58 33 49.3 ± 0.9	3142 ± 7	0.12 ± 0.03	4.9 ± 1.0	tentative
NGC 4151	13	DnA	12 10 32.58 ± 0.01	+39 24 21.1 ± 0.1	695.6 ± 0.3	0.009 ± 0.002	0.035 ± 0.007	tentative

Notes. [a] Error estimates associated with this quantity are discussed in Sect. 2.4. [b] All values obtained by Gaussian fits to the maser line(s) with the exception of NGC 4151 where a Gaussian fit would have been meaningless. In this case, the channel width of the spectrum was taken as a reliable upper limit for the uncertainty in the peak velocity, and the error on the line-integrated intensity has been computed assuming errors of 10 and 20% in the line intensity and width, respectively. [c] $L_{\rm H_2O}/[L_\odot] = 0.023 \times \int S\,dV/[{\rm Jy\,km\,s^{-1}}] \times D^2/[{\rm Mpc^2}]$.

3. Results

3.1. NGC 3556

NGC 3556 is a nearby[3] ($D \sim 12$ Mpc, 1″ is equivalent to ~60 pc) edge-on spiral galaxy with an FIR luminosity similar to that of the Milky Way ($L_{\rm FIR} \sim 10^{10}\,L_\odot$). The presence of a conspicuous radio halo (Irwin et al. 1999), prominent HI loops interpreted as expanding supershells (King & Irwin 1997), and extraplanar diffuse X-ray emission (Wang et al. 2003a) all indicate that NGC 3556 is undergoing an intense disk-halo interaction. At high resolution, the radio continuum emission is resolved into a number of discrete components, which form a partial ring around the HI kinematic center (Irwin et al. 2000; hereafter ISE). Although a radio core is absent, Chandra X-ray observation revealed an ultraluminous X-ray source close to the HI kinematic center and the 2 μm peak, which has a power law spectrum typical of an AGN (Wang et al. 2003a). A significant amount of dense molecular gas is present in the galaxy, as proved by ^{12}CO and HCN observations (Gao & Solomon 2004). Water maser emission has been detected, for the first time, with Effelsberg, in March 2002. The detection spectrum and three more single-dish spectra at subsequent epochs are shown in HPT (their Fig. 5).

In our VLA observations, we detected H₂O water maser emission at $V_{\rm LSR} \sim 738$ km s^{-1} with a peak flux density for the CnB and DnA arrays of ~13 and 27 mJy, respectively (Fig. 1). A Gaussian fit to the spectra indicates that the full width to half maximum (*FWHM*) of the maser feature is 8 ± 2 and

---

[3] The distance is taken from King & Irwin (1997) and is derived from the radial velocity corrected for the anisotropy of the 3 K cosmic microwave background.
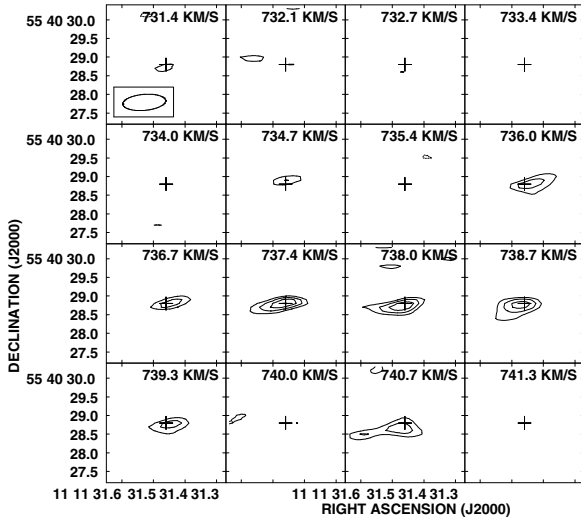

Fig. 1. The VLA CnB-array (blue solid line) and DnA-array (black solid line) water maser spectra of NGC 3556 taken in 2002 and 2006, respectively. Both spectra have a channel spacing of 0.7 km s^{-1}.

3.7 ± 0.3 km s^{-1}, yielding similar values for the isotropic maser luminosity for the two arrays, 0.29 and 0.28 $L_\odot$ (see Table 2).

Comparing the VLA CnB spectrum observed on September 28, 2002, with the spectrum taken with Effelsberg one day before (HPT; upper panel of their Fig. 5), we note that the peak flux density of the maser line observed by the VLA is less than half of what was observed with Effelsberg. The intensity of the VLA DnA spectrum is, instead, closer to the single-dish measurements. For all observations, taken with either Effelsberg or the VLA, the $V_{\rm LSR}$ velocity and linewidth of the maser features are consistent with each other.

Figures 2 and 3 show contour plots of those channels, which exhibit significant line emission and a moment-0 map (i.e. a map of the velocity-integrated intensity) in the velocity range 720–760 km s^{-1} obtained from the two CnB and DnA VLA datasets,

Fig. 2. Channel maps of the H_2O maser emission in NGC 3556 observed with the VLA CnB array. Contour levels are $-3, 3, 3.5, 4 \times 4$ mJy beam^{-1} (1σ rms = 4 mJy beam^{-1}). The cross indicates the position of the line peak.
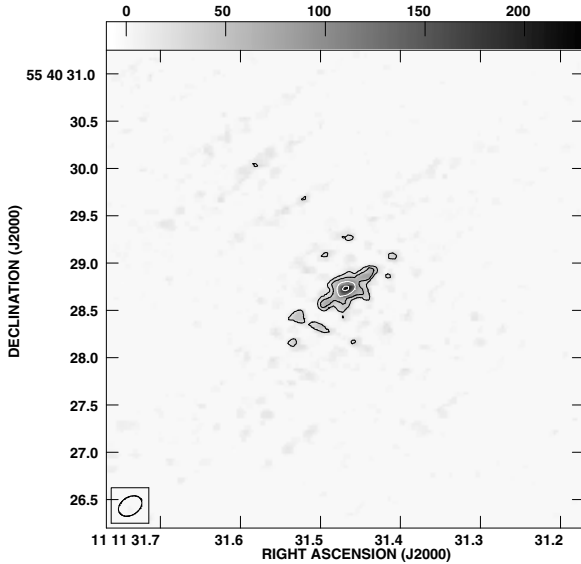
Fig. 3. Gray scale and contour plot of the total integrated intensity of the maser emission in NGC 3556 observed with the VLA DnA array. Integration was performed over the velocity interval 720–760 km s^{-1}. Contours: $-1, 1, 2, 4 \times 25$ mJy/beam/km s^{-1}. (1σ rms = 0.4 mJy/beam/km s^{-1}).

respectively. These maps indicate that the maser emission is slightly resolved both in space and velocity.

We fitted a two-dimensional Gaussian to the brightness distribution of the source in the VLA CnB channel map showing the most intense emission (from 737.4 to 738.7 km s^{-1} in Fig. 2, left panel) and find that the bulk of the emission arises from a spot of beam deconvolved dimensions of $\sim 0\farcs7 \times 0\farcs2$ at position $\alpha_{J2000} = 11^{h}11^{m}31\fs46$ and $\delta_{J2000} = 55°40'28\farcs8$. Tentative maser emission also seems to be present in a spot ~ 70 pc east of the main feature at a velocity $V_{LSR} = 740.7$ km s^{-1} and position $\alpha_{J2000} = 11^{h}11^{m}31\fs60$ and $\delta_{J2000} = 55°40'28\farcs5$ (Fig. 2). Additional weak spots might be present both in the CnB and DnA channel maps. These, however, are faint, arise from isolated channels and may be spurious.

Since VLA broad band 22 GHz data were not available, we produced CnB and DnA-array VLA continuum maps from the line-free channels. In both maps, no continuum emission was detected above a 1σ rms noise of ~ 0.5 mJy beam^{-1}. This result is consistent with the 1.4-GHz flux densities reported by ISE for the compact sources in the nuclear region of NGC 3556. Even the strongest source(s) of ISE remain(s) undetected in our maps indicating a nonthermal origin of the emission.
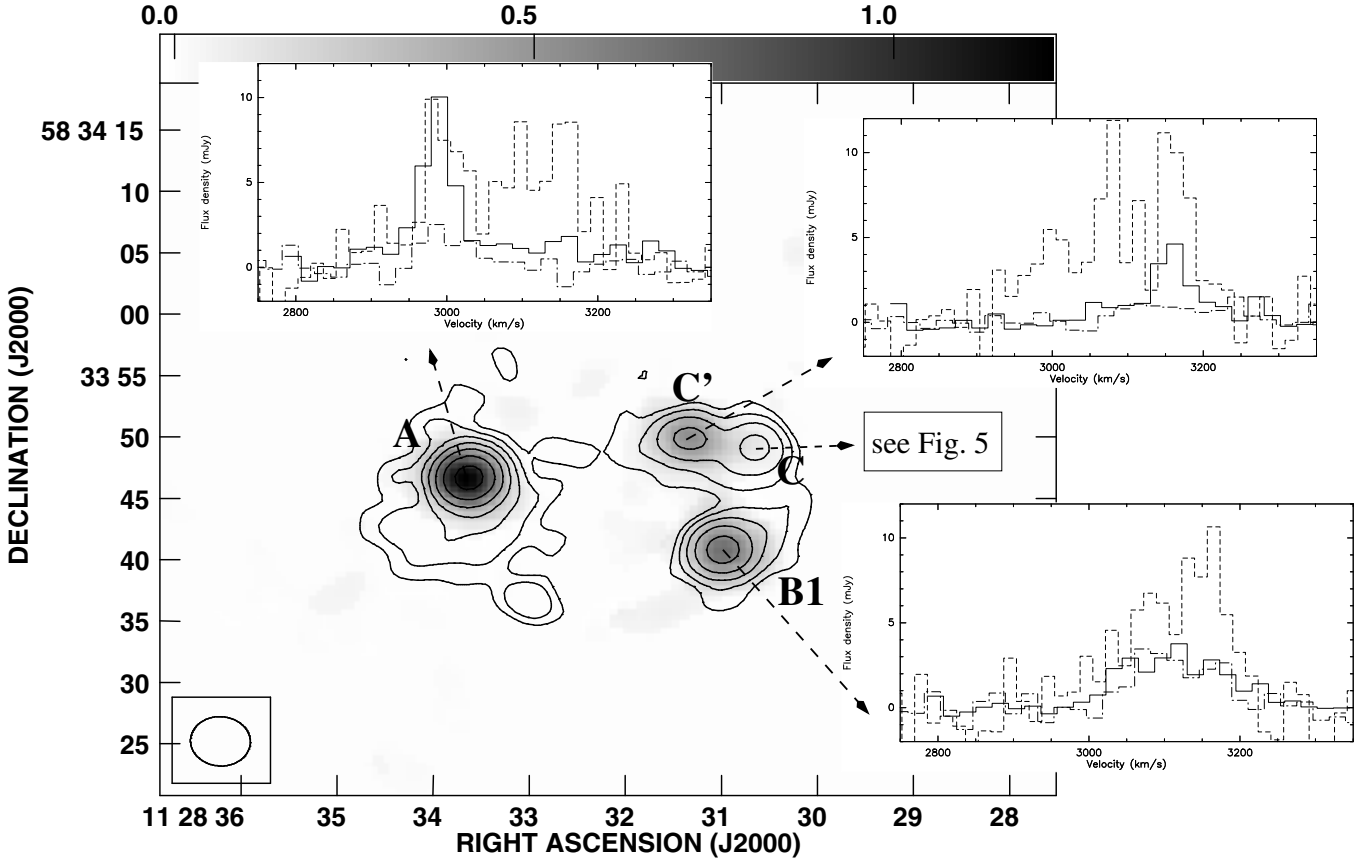
3.2. Arp 299

The extremely luminous infrared galaxy Arp 299 (Mkn 171)[4] is a merging system located at a distance of ~ 42 Mpc (Casoli et al. 1999). It is composed of three main regions of activity: the two galaxies IC 694 (**A**) and NGC 3690 (**B**; resolved at infrared and radio wavelengths into two components, **B1** and **B2**)[5], and the individual concentrations (**C** and **C'**) at the interface where IC 694 and NGC 3690 overlap (for a description of the system and for the nomenclature used, see, e.g., Neff et al. 2004; their Fig. 2). The system is rich in molecular gas (Casoli et al. 1999) and displays OH megamaser activity with an isotropic luminosity of $\sim 240 L_\odot$ (Baan 1985) apparently tracing a rotating disk in IC 694 (Baan & Haschick 1990; hereafter BH90). The presence of such a flattened rotating structure in IC 694 was subsequently also invoked by Polatidis & Aalto (2001) to explain its atomic (HI) and molecular (CO) gas velocity distribution. In March 2002, strong water megamaser emission was detected in the merging system Arp 299, with a total isotropic luminosity of $\sim 200 L_\odot$ (HPT). Later, preliminary results of our VLA A-array observations were reported in Tarchi et al. (2007b). They show that the water maser emission in the system is produced mainly by two spots associated with the innermost regions of IC 694 and NGC 3690. Tentative emission was seen in the overlapping region.

In a more thorough data reduction of the VLA A-array data, the scenario described in Tarchi et al. (2007b) is confirmed with higher confidence (see Fig. 4). Luminous maser emission is detected at two locations with coordinates $\alpha_{J2000} = 11^{h}28^{m}33\fs65$; $\delta_{J2000} = 58°33'46\farcs8$ and $\alpha_{J2000} = 11^{h}28^{m}30\fs99$; $\delta_{J2000} = 58°33'40\farcs7$, corresponding to the two brightest centers of activity in the system labeled A and B1 by Neff et al. (2004). The maser features have peak velocities of 2996 and 3112 km s^{-1}. Our recent VLA D-array data confirm emission in locations and velocities consistent, within the accuracies, with those resulting from the previously taken higher resolution VLA data. In particular, the tentative emission detected with the A-array in the overlap region is convincingly confirmed. Most of the emission originates from a bright spot (~ 4 mJy), peaks at a velocity of 3158 km s^{-1}, and has a position, $\alpha_{J2000} = 11^{h}28^{m}31\fs35$; $\delta_{J2000} = 58°33'49\farcs8$, coincident with the source C' of Neff et al. (2004). In Fig. 4 (large panel), we show the moment-zero map of the water maser emission in Arp299 observed by the VLA in its D configuration superposed on the 22-GHz uniformly-weighted VLA D-array radio continuum

---

[4] According to the NASA/IPAC Extragalactic Database (NED), the entire merger forms NGC 3690, while IC 694 is a less prominent galaxy 1' to the northwest. Here we follow the more traditional nomenclature that is commonly used in the literature.

[5] IR, radio, and X-ray observations all indicate that the putative nucleus of NGC 3690 is located at position B1. Source B2 is more prominent in the optical because it is less obscured than B1 at visible wavelengths and may be associated with a region vigorously forming massive stars (Alonso-Herrero et al. 2009, and references therein). Hereafter, we therefore consider B1 as the nucleus of NGC 3690.

Fig. 4. *Big panel*: moment-zero map (gray scale) of the water maser emission in the Arp299 system observed by the VLA in its D configuration superimposed on the 22-GHz uniformly-weighted VLA D-array radio continuum image (contours) of the system produced by using the line-free channels in the maser data cube. Contour levels are –1, 1, 2, 4, 8, 16, 32, 64 × 0.5 mJy beam^{-1} (1σ rms = 0.15 mJy beam^{-1}). *Small panels*: for each center of maser emission within the Arp299 system, spectra from Effelsberg (dashed line), VLA D-array (solid line), and VLA A-array (dash-dotted line) are shown, with a channel spacing of 17, 20, and 20 km s^{-1}, respectively.

image produced by using the line-free channels in the maser data cube. The spectra of the maser emitting regions observed with Effelsberg and the VLA, in its A and D configurations, are plotted in the smaller panels of the same figure. Location, line peak velocity, flux density, linewidth, and isotropic luminosity of the maser features are given in Table 2. Weaker emission (~1.8 mJy) in the overlap region is also detected at a position of $\alpha_{J2000} = 11^h 28^m 30\overset{s}{.}65$; $\delta_{J2000} = 58°33'49\overset{''}{.}3$ with a peak velocity of 3142 km s^{-1} and a line width of ~25 km s^{-1}. The location is coincident with the source C of Neff et al. (2004). For the sake of clarity, this feature is not included as a panel in Fig. 4, while it is shown, using a narrower, more-suitable y-axis scale, in Fig. 5.

3.3. NGC 4151

NGC 4151 is a grand-design, weakly barred spiral located at 13.3 Mpc (Braatz et al. 2004), which is known to host an active galactic nucleus (AGN). Although it is often classified as a type 1.5 Seyfert (Osterbrock & Koski 1976), its broad optical emission lines are variable and sometimes give a type 2 Seyfert spectrum (Sergeev et al. 2001). The equivalent hydrogen column density, inferred from the X-ray spectrum toward the nucleus, is also similar to what is found in typical Seyfert 2 galaxies ($N_H \sim 1.5 \times 10^{23}$ cm^{-2}, Wang et al. 2010). Radio observations of the nucleus show a linear radio structure (jet) approximately

3″5 (220 pc) in length, at a position angle (PA) 77° (Wilson & Ulvestad 1982). Carral et al. (1990) identified six discrete knots along the jet at 15 GHz, the strongest of which (peak flux density: 12.5 mJy/beam) has a flat spectral index that is consistent with the synchrotron self absorption associated with an AGN. Higher angular resolution VLBA and phased VLA observations at 1.4 GHz resolved the strongest knot into several components that appear to be associated with changes in the orientation of a faint highly collimated jet (diameter ≤1.4 pc), as it interacts with small gas clouds (Mundell et al. 2003). The identification of one of these components with the AGN is still uncertain. In Braatz et al. (2004), the detection of water maser emission with an isotropic luminosity of 0.7 $L_\odot$ was reported. The maser emission is primarily confined to two very narrow components, one at 692.4 km s^{-1} and the other at 1126.6 km s^{-1}, blushifted and redshifted, respectively, w.r.t. the systemic velocity of the galaxy, 995 km s^{-1}. For a channel spacing of 0.33 km s^{-1}, Gaussian fits of the emission lines yielded peak flux densities and linewidths of 36 and 53 mJy, and 1.2 and 1.5 km s^{-1} (*FWHM*), respectively.

Our VLA DnA spectra (Fig. 6, upper-right panel) indicate, in the first IF, the tentative presence of a narrow single-channel line at 695.6 km s^{-1} with a peak flux density of ~30 mJy for a channel spacing of 0.33 km s^{-1}, while no emission is detected in the second IF. The position of the putative emission feature is $\alpha_{J2000} = 12^h 10^m 32\overset{s}{.}58$ and $\delta_{J2000} = 39°24'21\overset{''}{.}1$. Assuming an upper limit for the uncertainty in the peak velocity of about one channel, 0.33 km s^{-1}, this feature, if real, is still offset
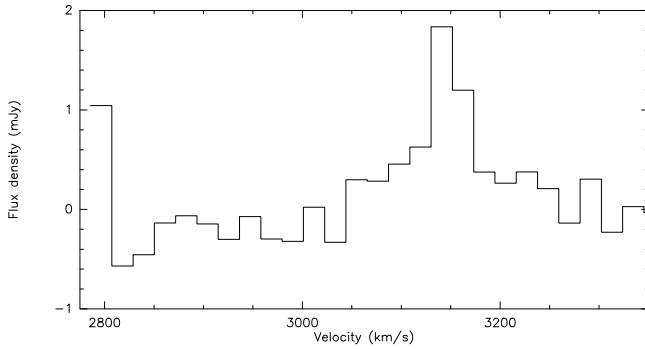
by $\sim$3 km s^{-1} from the one detected by Braatz et al. (2004). However, it may well belong to a group of variable features emitted in a narrow range of velocities. The indication of strong intrinsic variability in the NGC 4151 maser was indeed reported by Braatz et al. (2004).

The radio continuum contour map produced by using the line-free channels of the data cube is shown in the lower left hand panel of Fig. 6. A slightly-resolved source is detected at 22 GHz with position $\alpha_{J2000} = 12^h10^m32\overset{s}{.}58 \pm 0\overset{s}{.}01$ and $\delta_{J2000} = 39°24'21\overset{''}{.}1 \pm 0\overset{''}{.}1$ and a peak flux density of $\sim$15 mJy that is coincident in position, within the limits of accuracy ($\sim$0$\overset{''}{.}$07; see Sect. 2.4 and Table 1), both with the maser spot and with the putative AGN of NGC 4151 (e.g. Carral et al. 1990; Mundell et al. 2003; Ulvestad et al. 2005).

4. Discussion

4.1. Individual galaxies

4.1.1. NGC 3556

Since no continuum emission was detected in our 22-GHz map of NGC 3556, we use maps published in the literature. The main maser spot is possibly associated with the strongest compact source (hereafter referred to as CS-3556) shown in the 1.4-GHz VLA map of ISE (Fig. 7, lower panel) although with a relatively large uncertainty (the relative position error is of 0$\overset{''}{.}$1). Thus, the origin of the maser emission is closely related to the nature (AGN or star formation region) of CS-3556 and to the possible presence of an AGN.

While spectral index information on CS-3556 was not available, ISE concluded that the radio emission has a nonthermal origin and is due to a collection ($\sim$10) of supernova remnants (SNRs) that cannot be resolved by the synthesized beam. Although not mentioned by ISE, another possible explanation is that CS-3556 may actually be an individual bright SNR or radio supernova, like those found in M 82. Wang et al. (2003a) found an AGN candidate among the discrete X-ray sources detected with *Chandra* (hereafter labeled X-35). However, its position offset from both the H I kinematic center and the 2 μm peak (14$''$ ≡ 815 pc and 8$''$ ≡ 465 pc, respectively; see Fig. 7) and X-ray luminosity ($\sim$10^{39} erg s^{-1} in the 0.5–10 keV band), just at the lower limit of the Eddington luminosity, indicates a nature for X-35 that is more consistent with a luminous X-ray binary than with a putative AGN. A clear signature of an AGN is then missing. Furthermore, the source CS-3556 is confidently offset from X-35 and the H I peak (by 11$''$ and 8$''$, respectively), and,

in particular, from the 2 μm peak (the position which is known with an accuracy of $\sim$1$''$) by 5$''$. Most likely, CS-3556 is indeed a group of SNRs as proposed by ISE, or an isolated particularly bright SNR like those found in the nuclear regions of other starburst galaxies, rather than the galactic nucleus. That CS-3556 belongs to a chain of compact radio sources (Fig. 7) apparently tracing a partial ring or arm-like structure similar to those found in other galaxies and related to quasi-contemporary star formation triggered by a propagating density wave reinforces our conclusion.

Very recently, we obtained a deep 1.4-GHz MERLIN observation where we detected one continuum source in the nuclear region of NGC 3556 confidently associated with CS-3556. The source is relatively weak (with a flux density of 0.25 mJy) and extended in the naturally weighted image (Fig. 7, upper-left panel). When the source is imaged using uniform weighting, hence at a slightly higher resolution, the emission splits into two spots labeled CS-3556/A and CS-3556/B (Fig. 7, upper-right panel), most likely hinting at being composed of two galactic SNR-like sources, as suggested by ISE, or compact H II (CH II) regions. Future spectral index studies of these two sources may differentiate the thermal or nonthermal nature of the emission. In either case, this confirms the association between the maser and CS-3556 with higher position accuracy and, in particular, with CS-3556/A, the southwestern of the two continuum sources. Then, if our scenario is correct, the confident association of the H$_2$O maser with CS-3556/A indicates that the kilomaser in NGC 3556 is related to star formation as in the majority of the weak extragalactic masers.

The 50% flux density decrease observed between the Effelsberg spectrum on September 27, 2002 (30 mJy; HPT, their Fig. 3) and the VLA CnB profile (Fig. 1), obtained only a day later, hardly explicable in terms of variability, suggests that the maser feature observed with Effelsberg is a sum of a number of "weak" maser spots, which are resolved by the higher resolution of the VLA. Indeed, the channel maps (Fig. 2) indicate that the emission arises from more than one spot, even though only the strongest component is luminous enough to be confidently detected and to be present in more than one channel. The possibility that we are observing a collection of weak masers, the brightest of which has a luminosity of $\sim$0.3 $L_{\odot}$, once more favors the association with star formation activity.

Interestingly, the velocity of the maser line ($V_{LSR} = 738$ km s^{-1}) is redshifed by $\sim$40 km s^{-1} w.r.t. the systemic velocity of the galaxy ($V_{sys} = 699$ km s^{-1}, NED; $V_{LSR} - V_{HEL} = +5.90$ km s^{-1}). However, the maser line is located where the gas belonging to the H I disk has velocities of about 680 km s^{-1}, which is blueshifted w.r.t. the systemic ones (King & Irwin 1997). Therefore, the discrepancy between the observed and expected velocity is of the order of 60 km s^{-1}. When excluding an association with the galactic nucleus, as discussed before, this discrepancy can be explained by invoking gas motions in clouds (see, e.g. Surcis et al. 2009, for NGC 3256) or assuming that the masing gas belongs to a counter-rotating structure, an expanding supernova shell, or a starburst wind or outflow (see also Brunthaler et al. 2009, for a detailed analysis with respect to NGC 253). With the data presently available for NGC 3556, it is impossible to distinguish between these possibilities.

4.1.2. Arp 299

Simultaneous detection of luminous water maser emission in different regions of Arp 299 represents a unique case among the
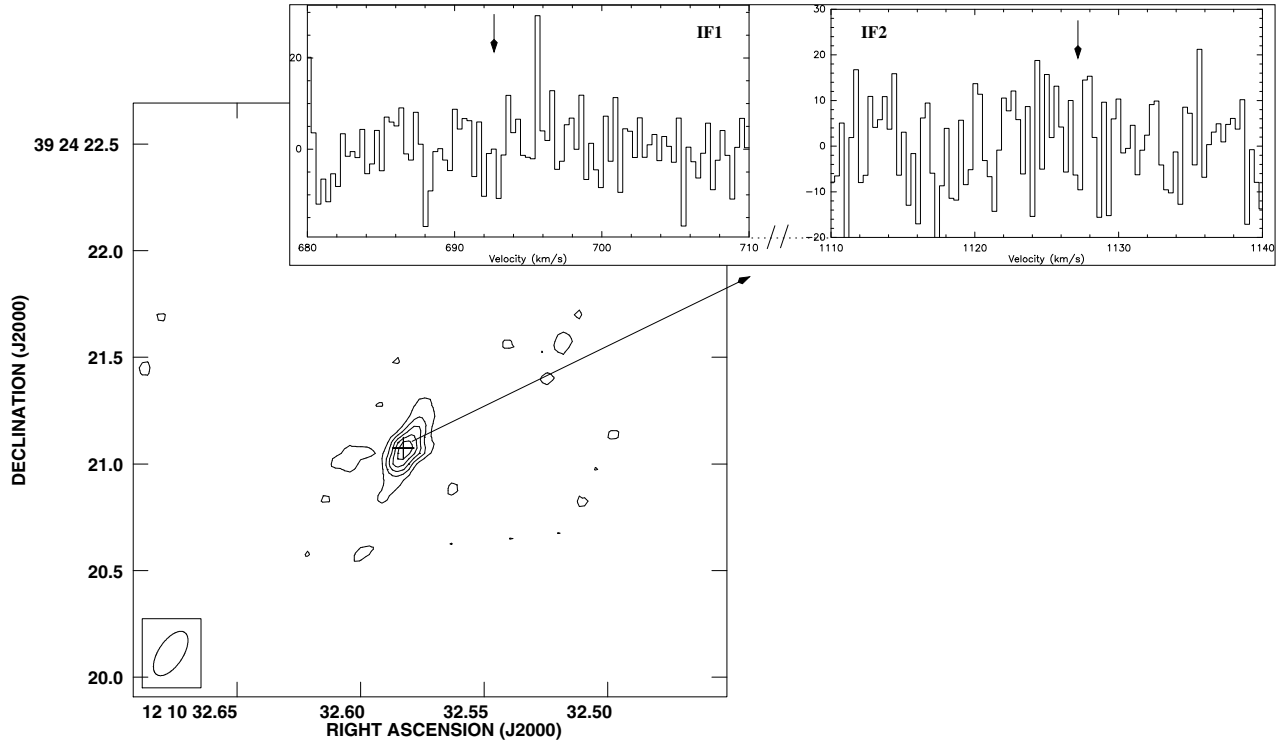
Fig. 6. *Lower-left panel*: naturally-weighted VLA DnA-array 22 GHz radio continuum contour map of NGC 4151 produced by using the line-free channels in the maser data cube. Contours: -1, 1, 2, 3, 4, 5×1.7 mJy (1σ rms $= 0.6$ mJy beam^{-1}). *Upper panels*: 22 GHz spectra from the IF1 (*left*) and IF2 (*right*) VLA DnA-array data cube. The two IFs sample the velocity ranges where narrow water maser lines (their velocities are marked by arrows) were detected with the GBT by Braatz et al. (2004). The systemic velocity of the galaxy is 995 km s^{-1}.

LIRG/ULIRG class of objects. Therefore, it provides an excellent opportunity to study origin and excitation mechanisms that form water masers in interacting galaxies and an important tool for understanding the entire Arp 299 merging system.

As previously reported (Sect. 3.2), one of the three main maser spots detected in Arp 299 is coincident with the nuclear region of IC 694. The higher spatial resolution map obtained from the VLA A-array indicates that the position of the maser is offset of $\sim 0\rlap{.}''2$ (≈ 40 pc at the distance of IC 694) to the northeast w.r.t. that of the nuclear radio continuum peak at 8 GHz (Neff et al. 2004). However, due to the relatively low signal-to-noise ratio of the VLA-A array observations, this result requires further confirmation. Another masing spot is located within a distance of $0\rlap{.}''1$ from the putative nucleus of NGC 3690 (Fig. 4). Then, a significant fraction of the emission is located in the overlapping region (the C + C'-complex), most of which is associated with the subcomponent labeled C', although weaker emission is present also at component C.

The velocities of the water masers are unusual when being compared with the H I (BH90) and CO (Casoli et al. 1999) velocity fields. In particular, the H₂O maser line associated with IC 694 should have a velocity around 3140 km s^{-1}, while it is detected at ~ 2990 km s^{-1}. The peak velocity (~ 3112 km s^{-1}) of the maser feature associated with the nucleus of NGC 3690 is instead more consistent with, although slightly redshifted to, what is expected from other gas tracers at the same location (~ 3050 km s^{-1}). Furthermore, more than one velocity component is present in the C+C'-complex.

The aforementioned discrepancies are, however, not surprising at all. The gas velocity field of Arp 299, both in its atomic and molecular component, is very complex and cannot be described by a composition of two independent, rotating disks representing the two main galaxies (e.g. BH90; Aalto et al. 1997). A simple picture to describe the behaviour of the H I and OH gas in Arp 299 has been proposed by BH90 where all the higher velocity gas belongs to IC 694 and that at lower velocity is related to NGC 3690. In this scenario, gas from both galaxies reaches the other galaxy to produce the apparent anomalies in the velocity field. Furthermore, gas from NGC 3690 and IC 694 also have components in C and C', respectively. While the maser found close to the nucleus of NGC 3690 can be safely associated with this galaxy, given its precise overlapping in position with the nuclear source and small difference in velocity, the maser apparently associated with IC 694, could instead be masing gas associated with the disk of NGC 3690, possibly amplifying emission from the nuclear (star-forming or AGN) region in IC 694. However, before drawing such a conclusion we should note that according to BH90 only the large scale velocity field is explained by the aforementioned simple model, while a closer look in front of the nuclear region of IC 694 shows several velocity components. In Fig. 8, we show a modified version of their figure (Fig. 11 in BH90) where such a description is summarized and where we have included the position and velocity of our maser to determine with which of the velocity components it can be associated. The proximity to the expanding structure in IC 694 introduced by BH90, makes an association between the water maser and this dynamical component likely. This structure, represented in both the HI absorption and OH maser emission data, is possibly a slab of material related to outflow phenomena due to superwinds produced in the AGN or regions with particularly enhanced star formation activity. Strong H I and OH outflows have been detected in several edge-on systems that share similarities to IC 694. We therefore think that the 2990 km s^{-1} feature is masing gas associated with IC 694.
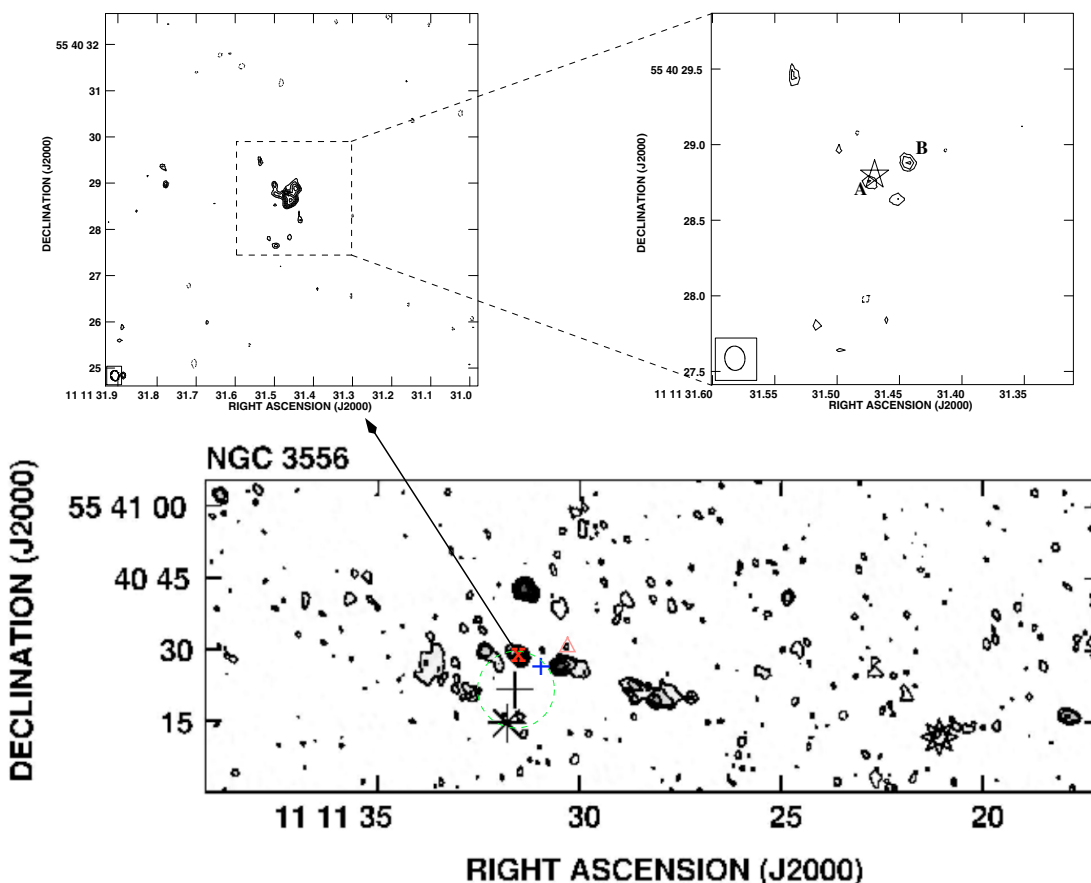
Fig. 7. *Lower large panel*: a VLA A-array map of the continuum emission of NGC 3556 at 20 cm (ISE). The asterisk identifies the optical center. The large black cross indicates the H I kinematic center given by King & Irwin (1997) with the relative error (dashed-line circle). The smaller blue cross near *the upper right corner* of the green dashed circle denotes the 2 μm peak. The pink triangle marks the position of *Chandra* source 35. The position of the water maser is indicated by the red X-mark. The multipointed star in the lower right edge indicates a position where some supernovae have been detected (see ISE). *Upper left panel*: naturally weighted contour image of the only compact nuclear radio continuum source, among those of ISE, detected in NGC 3556 at 1.4 GHz by MERLIN. Contours: –2.5, 2.5, 3, 3.5, 4, 4.5, 5 × 50 μJy/beam (1σ rms = 0.05 mJy beam^{-1}). *Upper right panel*: uniformly-weighted 1.4 GHz MERLIN contour image of the compact source. The star marks the water maser position. Contours: –3, 3, 3.5, 4 × 40 μJy/beam (1σ rms = 0.04 mJy beam^{-1}).
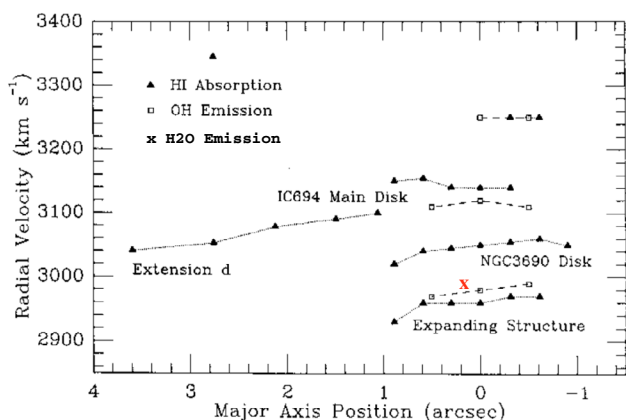
Fig. 8. A modified version of Fig. 11 of BH90 showing the H I and OH velocity components along the major axis (at position angle of ~45°) near the nucleus of IC 694. The red "X" marks the position and velocity the water maser feature detected by us in IC 694.

As already mentioned, our results can help determine the nature of the various objects constituting the Arp 299 system.

IC 694 The debate over the nature of A, the putative nucleus of IC 694, is ongoing. Based on the compact nature of the radio emission, some authors suggest there is an obscured AGN in A (e.g. Sargent & Scoville 1991; Lonsdale et al. 1992). From a comparison between the X-ray luminosity of A and B1, Ballo et al. (2004) deduce that both IC 694 and NGC 3690 host AGN activity. According to them, such X-ray intensity could not be accounted for by star formation alone. However, Zezas et al. (2003) argued against this interpretation. Many other authors indicate that the nuclear region of IC 694 is exhibiting particularly strong and compact nuclear star formation activity with no evidence for an AGN (e.g. Alonso-Herrero et al. 2009 and references therein).

One of the questions that arise when looking at the three water maser spectra of IC 694 (that of Effelsberg, VLA-A, and VLA-D; Fig. 4, upper-left inserted panel) is the difference in their peak fluxes. Variability can indeed be invoked to justify these flux changes. This seems to be supported by the comparison of the single-dish spectra taken with the 100-m Effelsberg telescope in November 2005 and in April 2007 (only 4 days before the VLA D-array measurements) shown in Fig. 9, where the maser line associated with IC 694 seems to experience an increase in flux density. The intensity of the maser in NGC 3690
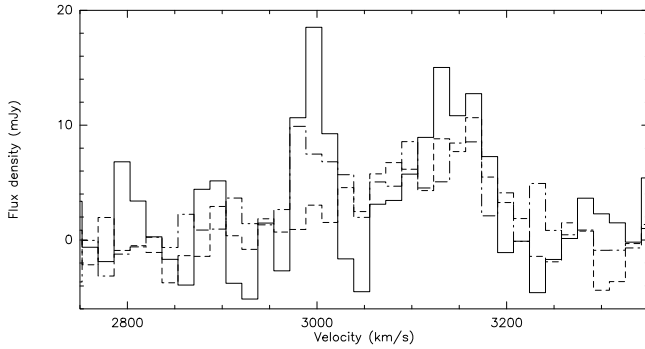
Fig. 9. Water maser spectra taken with the 100-m Effelsberg telescope on Nov. 2005, pointing towards putative nuclei of IC 694 (dash-dotted line) and NGC 3690 (dashed line), and on April 5, 2007 (4 days before the VLA D-array measurements) on a single pointing at intermediate distance between the nuclei (solid line). In this case, the Effelsberg 40″ beam covers the entire Arp 299 system.

does not change much. Given, however, the different characteristics of the measurements (with the older observation being sensitive and pointing at the individual nuclei, while the more recent spectrum is noisier and targets a middle point in the system), the variability scenario should be taken with caution.

An alternative option may also be viable. The lower resolution spectra (the November-2005 Effelsberg and VLA-D ones) have similar line flux densities and profiles. The spectrum taken with the VLA A-array is instead quite different. Although (as reported in Sect. 2) these observations were affected by bad weather that increased the noise level, the 60% reduction in flux density w.r.t. to the other spectra has to be considered as real. If the maser in IC 694 is associated with an AGN, as possibly suggested by its large interferometric brightness, ranging from 8 to 28 $L_\odot$ depending on the VLA array used, we would not expect to resolve its emission, and hence, to significantly lose flux, when passing from the D to the A array. If instead, the observed line is actually a collection of numerous maser spots associated with the intense star formation activity known to be present in IC 694 (e.g., Alonso-Herrero et al. 2009; and Pérez-Torres et al. 2009), at the resolution of the VLA A-array, we may start to resolve this group of spots. We could then be left with only the stronger ones, while the weaker may be below the detection threshold. Similar cases have been reported for a number of extragalactic kilomasers associated with star formation (Tarchi et al. 2002a, for NGC 2146; Surcis et al. 2009, for NGC 3256; present work, for NGC 3556). If this scenario is correct, the maser in IC 694 would be associated with star formation rather than an AGN. An additional hint of the possible "star-forming" nature of the maser is the 0″2 offset derived between the radio continuum peak in source A and the maser location (see above). This, of course, does not provide a definite answer to the question of AGN activity, especially since OH (mega)maser emission was found in source A (and only there in the entire system). Very recently, Ulvestad (2009) has reported on a study of the radio luminosities of the 25 continuum compact sources detected in the nuclear region of IC 694 with sensitive VLBI observations, concluding that the possibility that one of these sources is associated with an AGN cannot be ruled out.

For IC 694, we also compared the positions of the emission produced by the two maser species. The VLA study by BH90 indicates that the OH emission is coincident with the central peak of radio emission in IC 694, but the emission is extended. Furthermore, OH pumping requires that the molecular gas is located close to the nuclear FIR region. The spatial coincidence between the OH maser and the radio continuum peak has also been confirmed at higher resolution with MERLIN (Polatidis & Aalto 2000, 2001) and, tentatively, with the EVN (Klöckner & Baan 2002). The location of the water maser emission is also very close to the nuclear region although a small offset w.r.t. the radio continuum seems to be present (see previous paragraphs). Since the OH maser absolute position is not reported in Polatidis & Aalto (2000), Polatidis & Aalto (2001), and Klöckner & Baan (2002) and the alignment accuracy between our VLA A-array map and that of BH90 is limited to ∼0″2, the possible coincidence between the two masing regions cannot be ruled out. In any case, our result provides first evidence of strong maser emission from both molecules.

NGC 3690 Several attempts have been made to unveil any AGN activity within this galaxy. della Ceca et al. (2002), Zezas et al. (2003), and Ballo et al. (2004) using X-ray observations, García-Marín et al. (2006) through optical measurements, and Gallais et al. (2004) and Alonso-Herrero et al. (2009) with studies at infrared wavelengths, all strongly support the hypothesis that B1 is the true nucleus of NGC 3690 hosting an AGN. The detection of our water maser confirms this conclusion. The maser spot's location is coincident, within an accuracy of 0″1 (≈20 pc at a 42 Mpc distance), with the putative nucleus of the galaxy (B1). Furthermore, water masers found in association with AGN typically have luminosities >10 $L_\odot$ and are forming a collection of spots closely grouped around the nucleus, thus only seen as a single feature on the angular scale of the VLA. The maser in NGC 3690 follows these characteristics, has an isotropic luminosity of ∼20 $L_\odot$, is spatially unresolved with the VLA A-array (100 mas resolution), and does not show any order of magnitude variations in its overall integrated flux density. The presence of an AGN in NGC 3690 is also considered possible by very recent radio continuum VLBI observations performed by Ulvestad (2009).

C+C'-complex Another truly relevant result of our VLA observations is the detection of emission in the C+C'-complex. Given its noticeable properties, e.g. the high molecular mass and the conspicuous NIR emission, it has been suggested that this complex was a satellite galaxy taking part in the merger event (e.g. Casoli et al. 1989; Telesco et al. 1985; Nakagawa et al. 1989). However, BH90 concluded that it is not necessary to invoke a third galaxy in the system to justify the region C's properties. Our finding, the presence of H₂O kilomaser emission associated with the C-complex both in the subcomponents C' and, at a weaker level, C, favors vigorous star formation and does not provide any strong hint of an active nuclear core. The youth and intensity of this burst, as deduced from its exceptionally strong 22-GHz emission and the presence of a substantial population of (ultra-)compact/ultradense (UC/UD) H II regions (e.g., Alonso-Herrero et al. 2009), is remarkable. A similar case has recently been reported by Darling et al. (2008) for the Antennae system (NGC 4038/4039), where water kilomaser emission of ∼8 $L_\odot$ has been detected in the "interaction region" (IAR) offset from the nuclei of the two galaxies taking part in the merger. The emission arises from one spatially unresolved spot separated in velocity into two distinct features. The water kilomaser emission is similarly luminous in the Antennae and the C-complex of Arp 299. This further corroborates similar physical conditions, as already suggested by common properties like enhanced star formation, strong (N)IR emission, and the presence of several UD H II regions (Darling et al. 2008).

The Arp 299 and Antennae merging systems themselves are, however, quite different. Assuming a distance of 42 Mpc

for Arp 299 (see Sect. 3.2) and of 21 Mpc for the Antennae (Darling et al. 2008), the IR luminosity of the former (L_{IR} $\approx 5 \times 10^{11}$ $L_\odot$; Alonso-Herrero et al. 2000) is 5 times that of the latter (L_{IR} $\approx$ 10^{11} $L_\odot$; Sanders et al. 2003). Furthermore, the linear distance between the two galactic nuclei in the systems (IC 694/NGC 3690 and NGC 4038/4039) derived from interferometric radio maps are 5 (Neff et al. 2004) and 7 kpc (Neff & Ulvestad 2000), respectively. In general, the merger in Arp 299 is more advanced than in the Antennae (e.g. Sargent & Scoville 1991; Schulz et al. 2007). Since galaxy mergers are a very efficient means of fueling AGN (e.g., Combes 2001), the different stage of the mergers may account for the AGN activity in Arp 299 that is not detected in the Antennae. At the same time, since advanced mergers may result in burying AGN with high concentrations of obscuring material, the large nuclear obscuration would also favor very luminous maser emission. This would further explain our water maser detection in the nuclei of the two galaxies of Arp 299. No maser emission has been reported so far in either of the two nuclei of the Antennae. Indeed, the nucleus of NGC 4038 has been searched for water maser emission down to a luminosity detection threshold of ~1 $L_\odot$ (HPT), while there has been no mention in the literature of a similar search in the nucleus of NGC 4039.

4.1.3. NGC 4151

The maser line tentatively detected in IF1 comes from an unresolved spot coincident in position with the continuum peak detected in the line-free channel map. From its location this peak can be identified as the sub-component E of the radio knot C4 (labels are from Mundell et al. 2003, and references therein). While the debate on the exact location of the AGN in NGC 4151 is still going on, the most recent publications indicate that D, and in particular subcomponent D3, is the most promising candidate, based on the location and distribution of the H I absorption, the structure of the radio continuum (Mundell et al. 2003), and the high brightness temperature of the source (Ulvestad et al. 2005). According to Mundell et al. (2003), source E is instead the brightest knot of the radio counterjet that is located behind the H I absorbing layer. If this is the case, the kilomaser in NGC 4151 may be produced by an interaction between the radio jet and the interstellar medium (ISM). Indeed, indications of such an interaction between the radio jet and the clumpy ISM of NGC 4151 are reported by Mundell et al. (2003). NGC 4151 may then represent the second case of a nuclear kilomaser, just after M 51 (Hagiwara et al. 2001b). Similarities do exist between the two cases like the presence of redshifted and blushifted emission in the single-dish spectra, although the maser features in M 51 are broader than those in NGC 4151, hence more consistent with the linewidths found for the megamaser sources associated with radio jets. The strength, narrowness, and strong variability of the maser features favor instead an association with star formation activity that, with the present data, cannot be excluded.

4.2. Kilomasers revisited

In Table 3, we have summarized relevant results related to extragalactic H_2O kilomasers, in the context of their association with AGN, SNRs, or H II regions. We have a total of 32 kilomaser sources in 24 galaxies. Half (16) of these 32 kilomasers (labeled "SF") are confidently associated with star formation activity being either clearly off-nuclear or, like NGC 253 H_2O–1

and NGC 3556, coincident in position with sources in the nuclear region produced by star formation phenomena. For the 8 sources labeled with "SF(?)", the association with star formation is instead (only) the most likely option since it is based on qualitative considerations on the nuclear position of the maser emission, the absence of clear evidence of AGN activity in the host galaxy and/or the shape of the maser line profile (see e.g., Castangia et al. (2008), for NGC 520, Surcis et al. (2009), for NGC 3620).

For other 4 kilomasers (in NGC 2273, NGC 4051, NGC 4151, and NGC 4293, labeled with "AGN?") the origin of the maser emission has been instead plausibly related to AGN activity (although, also in this case, a validation is necessary), mainly because the nucleus of the galaxy hosting the maser emission is an AGN and/or the maser line profile resembles more that of the AGN-associated ones (see, e.g., Hagiwara et al. 2003, for NGC 4051; the present work for NGC 4151). Among the remaining sources, for 2 of them (in NGC 1106 and NGC 4527) both associations, AGN or star formation, are equally plausible (Braatz & Gugliucci 2008), while for the kilomaser in NGC 6300 the nature of the maser emission, so far, has never been discussed. Noticeably, the only kilomaser ever reported that is undoubtedly associated with an AGN (labeled with "AGN") and, in particular, with the nuclear radio jet, is the one in M 51 (Hagiwara et al. 2001b).

The question arises therefore wether there is a family of nuclear, AGN-associated, kilomasers. Are there intrinsic differences in the host galaxy that, in the absence of studies at high (<1″) spatial resolution, can allow us to distinguish between kilomasers associated with star formation and those associated with AGN activity? A possible suggestion is briefly introduced by Zhang et al. (2006) and, more recently, by Greenhill et al. (2008) in the broader framework of the association between maser phenomena and nuclear X-ray column density. Their general conclusion was that the distributions of kilomasers and megamasers are different, with the latter associated with galaxies with higher nuclear column densities. Half of the megamasers in their sample are Compton-thick, viz. N_H > 10^{24} cm^{-2}. In particular, Zhang et al. (2006) found that, for kilomasers, two groups were apparently present, one with nuclear column densities of 10^{21-22} cm^{-2} and another with nuclear column densities of >$10^{23.3}$ cm^{-2}. Furthermore, it was put forward that the few nuclear kilomasers have an average column density that is indistinguishable from those of the entire megamaser sample. In Fig. 10, we show an updated plot from Zhang et al. (2006) (their Fig. 6a), with the number of H_2O kilomasers as a function of nuclear column density derived from X-ray spectroscopy for all 19 kilomaser galaxies (Zhang et al. 2006: 12 galaxies) for which such information was available. From Fig. 10, it is clear that the lower average nuclear column density of kilomasers compared to that of megamasers is confirmed, while there is no evidence of the "bimodal" distribution of nuclear column densities within kilomasers. The value for the nuclear column densities is a continuous function that spans a range of values between $10^{21.08}$ cm^{-2} (M 82) and $10^{24.75}$ cm^{-2} (M 51; although the values for NGC 6300 and NGC 2273 are only lower limits). Indeed, as qualitatively suggested by Zhang et al. (2006), the kilomasers associated, or most likely associated, with AGN activity are found in galaxies with higher nuclear column densities (10^{23} cm^{-2} < N_H < 10^{25} cm^{-2}), different from those with a star-forming origin, which are found in galaxies with nuclear column densities <10^{23} cm^{-2}. The only exception is represented by the maser in NGC 253 that, despite being quite confidently associated with star formation (Hofner et al. 2006; Brunthaler et al. 2009),
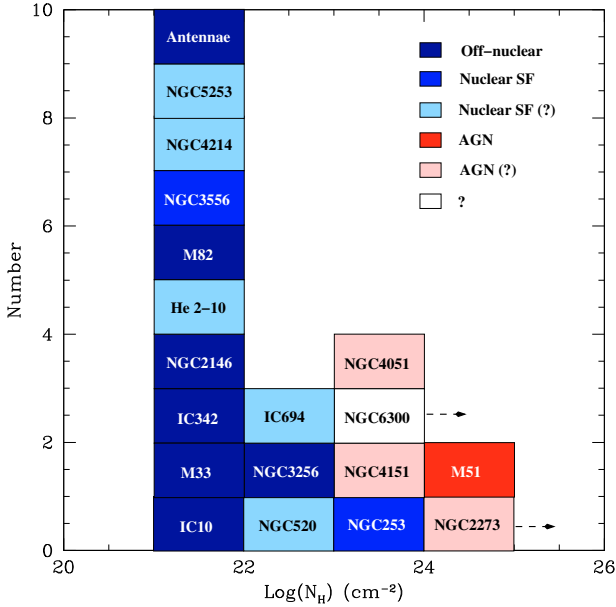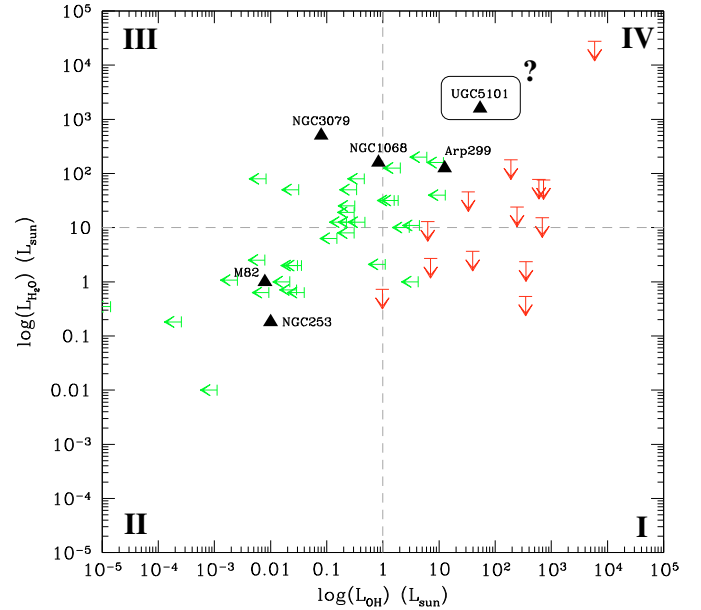
Fig. 10. Histogram showing the number of H_2O kilomaser galaxies as a function of their nuclear column density derived from X-ray spectroscopy. Due to the higher angular resolution, Chandra data are taken whenever possible (with the exception of NGC 4051 for which the XMM-derived column density value was preferred to that of Chandra because of the large uncertainties reported). Otherwise, the most recent measurements are used (see Table 4). The arrows for NGC 2273 and NGC 6300 indicate lower limits to the column densities. Each color indicates the association of the water maser emission with either star formation or AGN activity, and the degree of confidence in such an association.

Fig. 11. OH vs. H_2O maser luminosity including all sources where masers from both species have been searched for. Green arrows represent the galaxies hosting only H_2O maser emission, red arrows are those sources hosting only OH maser emission, and filled triangles are galaxies where both H_2O and OH masers have been detected. Upper limits for the undetected maser species are set to the detection luminosity threshold (3σ) of the survey in that maser transition. The dashed lines indicate the separation between kilomaser and megamaser regimes as found in the literature (for H_2O masers, see Sect. 1; for OH masers, see Henkel & Wilson 1990). The question mark associated with the position in the plot of UGC 5101 is explained in Sect. 4.3.

is found in a galaxy with relatively high column density (2×10^{23} cm^{-2}). According to this view, kilomasers like those in NGC 6300 or NGC 2273, for which the nature of the emission is still uncertain, could be speculatively associated with AGN activity because of the high nuclear column density. Interestingly, very recent results indicate that the latter maser source is indeed associated with an accretion disk around the central engine of the galaxy (Greene et al. 2010). Unfortunately, for five kilomaser galaxies (NGC 1106, NGC 3359, NGC 3620, NGC 4293, and NGC 4527), no information on column densities could be obtained. Future observations of these targets by $XMM-Newton$ and *Chandra* would be desirable.

If our picture is correct, then the presence of a family of nuclear kilomasers associated with AGN activity is possible. One of the distinguishing characteristics may indeed be the higher obscuration present around nuclear engines that we infer from the nuclear X-ray column densities. Since our discussion only involves nuclear X-ray column densities, we cannot (and do not want to) investigate the relation between the kilomaser phenomenon and the X-ray absorption in off-nuclear kilomaser regions. However, these detections originate from single-dish searches for water maser emission that, for more distant objects, cover the entire body of the target galaxy or, for the nearer ones, most of the galactic disk extent, including the nuclear regions. Hence, the lack of nuclear maser emission in these galaxies having relatively low nuclear X-ray column densities reinforces our supposition.

According to our results, the typical distinction between two classes of extragalactic water maser sources, kilo- and megamasers, based on a sharp isotropic luminosity edge traditionally

set to 10 $L_\odot$ should, in our opinion, be revised. While it is quite safe to state that the upper end of the water maser luminosity function is populated exclusively by maser sources associated with AGN activity, a mixture of masers associated with either star formation or AGN activity seems to be present at lower luminosities. In particular, since maser isotropic luminosities, especially for those AGN-related, may be strongly dependent on orientation effects, the existence of relatively low-luminous AGN-related masers may be justified. If necessary, a more proper way to distinguish between water masers should thus be related to the origin of the emission associated to either one of the aforementioned forms of activity.

4.3. On the H_2O/OH relation

Table 5 lists all sources where maser emission from either H_2O or OH, or both, has so far been reported in the literature[6]. Out of the 173 sources of Table 5, 85 host water maser emission, and 94 have OH maser emission detected. Six sources overlap between the two groups since they show maser emission from both molecular species. Unfortunately, not all sources that host maser emission from either one of the maser species have also been searched for emission from the other molecule. In Fig. 11, we show a plot with the water and OH maser isotropic luminosities (measured values for detections or 3σ upper limits in case of non

---

[6] Additional 50 unpublished galaxies, where 22 GHz water emission has been recently detected, are listed on the "Megamaser Cosmology project" homepage. However, no luminosity information has so far been reported, so these sources are not included in our list.

Table 3. Properties of extragalactic 22 GHz H_2O kilomasers and their potential association with AGN, SNR, or HII regions.

Source	Distance[a] (Mpc)	L_{H_2O}[a] $L_\odot$	Association[b]	Notes	References
IC 10–NW	1.2	0.02	SF	Molecular cloud	(Becker et al. 1993)
IC 10–SE		0.15	SF	HII region	(Becker et al. 1993)
NGC 253 H_2O–1	3.0	0.15	SF	SNR	(Hofner et al. 2006; Brunthaler et al. 2009)
NGC 253 H_2O–2		0.02	SF	Star-forming region	(Henkel et al. 2004)
NGC 520	30.0	1.00	SF(?)	SNR	(Castangia et al. 2008)
M 33-IC 133	0.7	0.32	SF	HII region	(Churchwell et al. 1977)
M 33-19		0.03	SF	HII region	(Huchtmeier et al. 1978)
M 33-50		0.02	SF	HII region	(Huchtmeier et al. 1980; Brunthaler et al. 2006)
NGC 1106	57.8	8.0	?		(Braatz & Gugliucci 2008)
IC 342	2.0	0.01	SF	Star-forming region	(Tarchi et al. 2002b)
NGC 2146–A	14.5	0.50	SF	UCHII region	(Tarchi et al. 2002a)
NGC 2146–B		1.20	SF	UCHII region	(Tarchi et al. 2002a)
NGC 2273	24.5	7.00	AGN(?)	Compton-thick	(Zhang et al. 2006)
He 2-10	10.5	0.68	SF(?)		(Darling et al. 2008)
M 82-NE	3.7	0.02	SF	HII regions	(Hagiwara 2007)
M 82-SW	3.7	0.10	SF	HII regions	(Hagiwara 2007)
NGC 3256–N	37.4	1.00	SF		(Surcis et al. 2009)
NGC 3256–S		2.40	SF		(Surcis et al. 2009)
NGC 3359	13.5	0.7	SF(?)		(Braatz & Gugliucci 2008)
NGC 3556	12.0	1.00	SF	SNR	present work
NGC 3620	22.4	2.10	SF(?)		(Surcis et al. 2009)
Arp 299–A	42.0	7.9	SF(?)		present work
Arp 299–C'		3.4	SF		present work
Antennae	20.0	8.2	SF(?)		(Darling et al. 2008)
NGC 4051	10.0	2.00	AGN(?)		(Hagiwara et al. 2003)
NGC 4151	13.5	0.63	AGN(?)		(Braatz et al. 2004; present work)
NGC 4214	2.9	0.028	SF(?)		(Darling et al. 2008)
NGC 4293	11.9	1.26–5.01	AGN(?)	jet(?)	(Kondratko et al. 2006)
NGC 4527	23.1	4.0	(?)		(Braatz & Gugliucci 2008)
M 51	10.0	0.63	AGN	Radio jet	(Hagiwara et al. 2001b)
NGC 5253	3.3	0.021	SF(?)		(Darling et al. 2008)
NGC 6300	15.0	3.16	?		(Greenhill et al. 2003)

Notes. [a] The isotropic luminosity is that of individual maser spots when the emission is spatially resolved. Otherwise, the full luminosity is taken from a single-dish measurement. For the sources not studied in the present work, distances and luminosities are taken from HPT. [b] The reported labels identify the maser association: "SF" and "AGN" indicate that interferometric measurements have confidently associated the maser emission with either star formation activity or an active galactic nucleus. A "?" sign is added to the favourite option, if there exist still some doubts. For unexplored sources, only a "?" sign is given.

detections), mainly derived from single-dish measurements, for those galaxies (51) that were searched for maser emission from both species. The plot can be summarized as follows:

– 32 galaxies show only water maser emission;
– 13 galaxies show only OH maser emission;
– no OH megamaser also shows H_2O kilomaser emission (quadrant I);
– 6 sources show maser emission from both molecules. In particular, the two well-known starburst galaxies NGC 253 and M 82 show kilomaser emission from H_2O and OH (quadrant II), the two water megamaser galaxies NGC 3079 and NGC 1068 also host an OH kilomaser (quadrant III), and Arp 299 and UGC 5101 (doubts, however, on the result for this galaxy are described later in this section) show megamaser emission from both molecules (quadrant IV).

Being aware that statistics may be affected by the different and/or insufficient sensitivities of maser searches and by possible variations in the maser features, we try in the following to provide a possible interpretation of these results. Despite our warning on using a strict isotropic luminosity threshold to infer the origin of water maser emission (see previous section), in the following

for consistency with past works (see e.g. Surcis et al. 2009, and references therein), we necessarily have to use 10 and 1 $L_\odot$ as isotropic luminosities to distinguish between the kilomaser and megamaser regime for H_2O and OH, respectively. According to this classification, 95% (89/94) are OH megamasers in all the galaxies where OH maser emission has been found. For water masers, 73% (62/85) are megamasers. Figure 11 indicates that, for the subsample of galaxies searched for both maser species, most of the OH detections (14 out of 19) are megamasers (with NGC 1068 and NGC 4355 having luminosities very close to the upper limit for kilomasers). Since very luminous masers are always found in AGN, the distances for the OH maser galaxy subsample is, on average, higher than for the H_2O masers, where a relatively lower number of megamaser sources (21 out of 39) are present. Due to the different average distance of the samples, the luminosity detection threshold is typically higher for water maser searches in OH-masing galaxies than for OH searches in H_2O-maser hosts. This may partly justify the results for quadrants I to III: no OH megamaser with a detected H_2O kilomaser but 4 OH kilomasers, indeed the closest four galaxies of the OH subsample, also detected in the water maser line. This suggests that weak masers from both species should indeed coexist in the same object (although possibly not at the very same

Table 4. Nuclear X-ray absorbing column densities of extragalactic H_2O kilomaser galaxies[*]. This table is an updated version of that presented by Zhang et al. (2006).

Source	Type[a]	Telescope[b]	Epoch[c]	N_H $(10^{23}$ cm$^{-2})$	References
IC 10	X-1	C	2003.03.12	$0.06^{+0.002}_{-0.0008}$	Bauer & Brandt (2004)
NGC 253	SBG	B	1996.11.29	$0.12^{+0.03}_{-0.04}$	Cappi et al. (1999)
		C	1999.12.16	$2.0^{+1.3}_{-0.9}$	Weaver et al. (2002)
NGC 520	X-12	C	2003.01.29	0.23	Read (2005)
		R	2003.01.29	0.029	Henriksen & Cousineau (1999)
M 33		A	1993.07	$0.016^{+0.002}_{-0.002}$	Takano et al. (1994)
	X-8	X	2000–2002	$0.019^{+0.005}_{-0.005}$	Foschini et al. (2004)
NGC 1106	–	–	–	–	–
IC 342		A	2000.02.24	$0.084^{+0.042}_{-0.042}$	Kubota et al. (2002)
	X-21	X	2001.02.11	$0.087^{+0.013}_{-0.025}$	Kong (2003)
NGC 2146	SBG	A	1997.03.26	$0.021^{+0.022}_{-0.011}$	della Ceca et al. (1999)
NGC 2273	S2, C	B	1997.02.12	>100	Maiolino et al. (1998)
		X	2003.09.05	≥18	Guainazzi et al. (2005)
He 2-10	BCD	R	1992.05.14	0.0084−0.047	Méndez et al. (1999)
		C	...	$0.0123^{+0.002}_{-0.002}$	Ott et al. (2005)
M 82[d]	SBG	B	1997.12.06	$0.058^{+0.014}_{-0.015}$	Cappi et al. (1999)
		X	2001.05.06	$0.017^{+0.018}_{-0.016}$	Stevens et al. (2003)
		C	2002	0.012	Strickland et al. (2004)
NGC 3256		X	2001.12.15	0.015	Jenkins et al. (2004)
	X-7 (N)	C	2000.01.05	0.01	Lira et al. (2002)
	X-8 (S)	C	2000.01.05	0.5	Lira et al. (2002)
NGC 3359	–	–	–	–	–
NGC 3556	X-35	C	2001.09.08	$0.03^{+0.017}_{-0.009}$	Wang et al. (2003b)
NGC 3620	–	–	–	–	–
Arp 299 (A; IC 694)	X-16	C		$0.119^{+0.102}_{-0.074}$	Zezas et al. (2003)
Arp 299 (C'; overlap)	X-8	C		???	Zezas et al. (2003)
Antennae	X-25 (NGC 4038)	C	1999.12.01	$0.107^{+0.036}_{-0.042}$	Zezas et al. (2002)
	X-29 (NGC 4039)	C	1999.12.01	0.014	Zezas et al. (2002)
NGC 4051	S1/1.5	A	1993.04.25	$0.045^{+0.035}_{-0.035}$	George et al. (1998)
		C	2000.04.25	~0.01	Collinge et al. (2001)
		X	2001.05.16	~3.6	Pounds et al. (2004)
NGC 4151	S1.5	A	1993.12.07	$0.635^{+0.041}_{-0.035}$	George et al. (1998)
		A, B	1999–2000	$2.0^{+0.1}_{-0.1}$	Schurch & Warwick (2002)
		C	...	1.5	Wang et al. (2010)
NGC 4214	BCD	C	...	$0.101^{+0.014}_{-0.011}$	Ott et al. (2005)
NGC 4293	LINER	R	...	see Table 3	HEASARC
NGC 4527	–	–	–	–	–
M 51	S2, C	A	1993.05.11	$7.5^{+2.5}_{-2.5}$	Bassani et al. (1999), Terashima et al. (1998)
		B	2000.01.18	56^{+40}_{-16}	Fukazawa et al. (2001)
NGC 5253	Dwarf SBG	C	...	$0.101^{+0.003}_{-0.003}$	Ott et al. (2005)
NGC 6300	S2, C?	RX	1997.02	>100	Leighly et al. (1999)
		B	1999.08	$2.10^{+0.10}_{-0.10}$	Guainazzi et al. (2002)
		X	2001.03.02	$2.15^{+0.08}_{-0.09}$	Matsumoto et al. (2004)

Notes. [*] *Chandra* and *XMM-Newton* results are given whenever possible. For sources not observed by these satellites most recent (but usually older) results are quoted. [a] Type of nuclear activity. In the absence of a starburst and a prominent nuclear source, the X-ray source (e.g. X-1 or X-8) is given. BCD: Blue Compact Dwarf; SBG: StarBurst Galaxy; S2: Seyfert 2; LINER: Low-Ionization Nuclear Emission Line Region; ULIRG: UltraLuminous InfraRed Galaxy; FRII: Fanarov-Riley type II galaxy; C: Compton-thick, i.e. $N_H \gtrsim 10^{24}$ cm^{-2}; C?: possibly varying between Compton-thick and Compton-thin. [b] A: *ASCA*; B: *BeppoSax*; C: *Chandra*; R: *ROSAT*; RX: *RXTE*; X: *XMM-Newton*. [c] Year, month and day. [d] For NGC 3034 (M 82), lacking a well defined nucleus, the *Chandra* data refer to the diffuse halo component.

location), similar to what happens in galactic star-forming regions. Possibly, only a selection effect of the sensitivity of the surveys has so far limited the number of detections of the contemporary presence of kilomasers from both species to a few.

In our study, only two galaxies show megamaser emission from both molecular species, Arp 299 and UGC 5101. However, the OH megamaser detection in UGC 5101 reported by Martin (1989) has never been confirmed, and doubts were raised by the non-detection obtained later by Baan et al. (1992). Without a confirmation of the OH megamaser line in UGC 5101, we consider the system Arp 299 as the only clear case with detected megamaser emission from both molecular species. But then, what is causing this apparent lack of "double" detections? To answer this question, a more systematic approach (parallel surveys to detect H_2O maser emission in OH maser galaxies, and viceversa) and a more detailed study of the, so far, unique case, IC 694, are necessary.

5. Conclusions

From the results of our interferometric observations on three extragalactic water maser galaxies and by more extended studies of water (and OH) maser sources, we can draw the following main conclusions.

- The kilomaser in NGC 3556 has a star formation origin associated with a compact radio continuum source, possibly identified as a supernova remnant or radio supernova.
- The megamaser in Arp 299 originates in three distinct regions associated with the nuclear regions of the two merging galaxies, NGC 3690 and IC 694, and in their region of interaction.
- Our study on Arp 299 confirms the likely presence of an AGN in the nucleus of NGC 3690. Without ruling out the possibility for AGN activity in IC 694, our outcome instead favors an association for the maser in this galaxy with an expanding structure possibly related to the extreme star formation activity taking place in the innermost region of the galaxy.
- The kilomaser in NGC 4151 originates in the nuclear region. Its association with the AGN, known to be present in the galaxy; cannot, however, be confidently assessed because we only tentatively detect one of the two maser features in our maps. The known variability of the two line features is possibly the main cause of our partial detection.
- Kilomasers are mostly associated with massive star formation, although a number of them are credibly related to low-luminosity AGN activity. The nuclear X-ray column density for the former type is typically lower than for the AGN-associated candidates, strengthening the possibility of there being two distinct classes. Given the low-luminosity of some of the maser sources associated with AGN, however, our study reinforces the conviction that a distinction between SF- and AGN-associated water masers based on a sharp isotropic luminosity threshold is not proper and instead requires case studies of individual systems to be assessed.
- A thorough analysis of the interplay between extragalactic maser emission from H_2O and OH is affected by how few objects were searched for both transitions. Nevertheless, our study indicates that, as expected, weaker maser emission from both molecular species can indeed be present in the same object, most likely because of the association of such emission with star formation processes. Only one case, that of Arp 299, is found to host megamaser emission from both

molecules. This case indeed deserves to be studied in even more detail.

References

Aalto, S., Radford, S. J. E., Scoville, N. Z., & Sargent, A. I. 1997, ApJ, 475, L107
Alonso-Herrero, A., Rieke, G. H., Rieke, M. J., & Scoville, N. Z. 2000, ApJ, 532, 845
Alonso-Herrero, A., Rieke, G. H., Colina, L., et al. 2009, ApJ, 697, 660
Baan, W. A. 1985, Nature, 315, 26
Baan, W. A., & Haschick, A. 1990, ApJ, 364, 65 (BH90)
Baan, W. A., Haschick, A., & Henkel, C. 1992, AJ, 103, 728
Baars, J. W. M., Genzel, R., Pauliny-Toth, I. I. K., & Witzel, A. 1977, A&A, 61, 99
Ballo, L., Braito, V., Della Ceca, R., et al. 2004, ApJ, 600, 634
Bassani, L., Dadina, M., Maiolino, R., et al. 1999, ApJS, 121, 473
Bauer, F. E., & Brandt, W. N. 2004, ApJ, 601, L67
Becker, R., Henkel, C., Wilson, T. L., & Wouterloot, J. G. A. 1993, A&A, 268, 483
Braatz, J. A., & Gugliucci, N. E. 2008, ApJ, 678, 96
Braatz, J. A., Henkel, C., Greenhill, L. J., Moran, J. M., & Wilson, A. S. 2004, ApJ, 617, L29
Brunthaler, A., Henkel, C., de Blok, W. J. G., et al. 2006, A&A, 457, 109
Brunthaler, A., Castangia, P., Tarchi, A., et al. 2009, A&A, 497, 103
Cappi, M., Palumbo, G. G. C., Pellegrini, S., & Persic, M. 1999, Astron. Nachr., 320, 248
Carral, P., Turner, J. L., & Ho, P. T. P. 1990, ApJ, 362, 434
Casoli, F., Combes, F., Augarde, R., Figon, P., & Martin, J. M. 1989, A&A, 224, 31
Casoli, F., Willaime, M.-C., Viallefond, F., & Gerin, M. 1999, A&A, 346, 663
Castangia, P., Tarchi, A., Henkel, C., & Menten, K. M. 2008, A&A, 479, 111
Churchwell, E., Witzel, A., Huchtmeier, W., et al. 1977, A&A, 54, 969
Collinge, M. J., Brandt, W. N., Kaspi, S., et al. 2001, ApJ, 557, 2
Combes, F. 2001, Astrophys. Space Sci. Suppl., 277, 29
Darling, J., Brogan, C., & Johnson, K. 2008, ApJ, 685, L39
della Ceca, R., Griffiths, R. E., Heckman, T. M., Lehnert, M. D., & Weaver, K. A. 1999, ApJ, 514, 772
della Ceca, R., Ballo, L., Tavecchio, F., et al. 2002, ApJ, 581, L9
Foschini, L., Rodriguez, J., Fuchs, Y., et al. 2004, A&A, 416, 529
Fukazawa, Y., Iyomoto, N., Kubota, A., Matsumoto, Y., & Makishima, K. 2001, A&A, 374, 73
Gallais, P., Charmandaris, V., Le Floc'h, E., et al. 2004, A&A, 414, 845
Gao, Y., & Solomon, P. M. 2004, ApJS, 152, 63
García-Marín, M., Colina, L., Arribas, S., Alonso-Herrero, A., & Mediavilla, E. 2006, ApJ, 650, 850
George, I. M., Turner, T. J., Netzer, H., et al. 1998, ApJS, 114, 73
Greene, J. E., Peng, C. Y., Kim, M., et al. 2010, ApJ, 721, 26
Greenhill, L. J., Kondratko, P. T., Lovell, J. E. J., et al. 2003, ApJ, 582, L11
Greenhill, L. J., Tilak, A., & Madejski, G. 2008, ApJ, 686, L13
Guainazzi, M., Matt, G., Fiore, F., & Perola, G. C. 2002, A&A, 388, 787
Guainazzi, M., Fabian, A. C., Iwasawa, K., Matt, G., & Fiore, F. 2005, MNRAS, 356, 295
Hagiwara, Y. 2007, AJ, 133, 1176
Hagiwara, Y., Diamond, P. J., Nakai, N., & Kawabe, R. 2001a, ApJ, 560, 119
Hagiwara, Y., Henkel, C., Menten, K. M., & Nakai, N. 2001b, ApJ, 560, L37
Hagiwara, Y., Diamond, P. J., Miyoshi, M., Rovilos, E., & Baan, W. 2003, MNRAS, 344, L53
Henkel, C., & Wilson, T. L. 1990, A&A, 229, 431
Henkel, C., Tarchi, A., Menten, K. M., & Peck, A. B. 2004, A&A, 414, 117
Henkel, C., Peck, A. B., Tarchi, A., et al. 2005, A&A, 436, 75 (HPT)
Henriksen, M., & Cousineau, S. 1999, ApJ, 511, 595
Hofner, P., Baan, W. A., & Takano, S. 2006, AJ, 131, 2074
Högbom, J. A. 1974, A&AS, 15, 417
Huchtmeier, W. K., Witzel, A., Kuehr, H., Pauliny-Toth, I. I., & Roland, J. 1978, A&A, 64, L21
Huchtmeier, W. K., Richter, O., Witzel, A., & Pauliny-Toth, I. 1980, A&A, 91, 259

Irwin, J. A., English, J., & Sorathia, B. 1999, AJ, 117, 2102
Irwin, J. A., Saikia, D. J., & English, J. 2000, AJ, 119, 1592 (ISE)
Jenkins, L. P., Roberts, T. P., Ward, M. J., & Zezas, A. 2004, MNRAS, 352, 1335
King, D., & Irwin, J. A. 1997, New Astron., 2, 251
Klöckner, H. R., & Baan, W. A. 2002, in Cosmic Masers: From Proto-Stars to Black Holes, ed. V. Migenes, & M. J. Reid, IAU Symp., 206, 430
Kondratko, P. T., Greenhill, L. J., Moran, J. M., et al. 2006, ApJ, 638, 100
Kong, A. K. H. 2003, MNRAS, 346, 265
Kubota, A., Done, C., & Makishima, K. 2002, MNRAS, 337, L11
Leighly, K. M., Halpern, J. P., Awaki, H., et al. 1999, ApJ, 522, 209
Lira, P., Ward, M., Zezas, A., Alonso-Herrero, A., & Ueno, S. 2002, MNRAS, 330, 259
Lonsdale, C. J., Lonsdale, C. J., & Smith, H. E. 1992, ApJ, 391, 629
Maiolino, R., Salvati, M., Bassani, L., et al. 1998, A&A, 338, 781
Martin, J. 1989, Ph.D. Thesis, Université de Paris
Matsumoto, C., Nava, A., Maddox, L. A., et al. 2004, ApJ, 617, 930
Méndez, D. I., Esteban, C., Filipović , M. D., et al. 1999, A&A, 349, 801
Mundell, C. G., Wrobel, J. M., Pedlar, A., & Gallimore, J. F. 2003, ApJ, 583, 192
Nakagawa, T., Nagata, T., Geballe, T. R., et al. 1989, ApJ, 340, 729
Neff, S. G., & Ulvestad, J. S. 2000, AJ, 120, 670
Neff, S. G., Ulvestad, J. S., & Teng, S. H. 2004, ApJ, 611, 186
Osterbrock, D. E., & Koski, A. T. 1976, MNRAS, 176, 61P
Ott, J., Walter, F., & Brinks, E. 2005, MNRAS, 358, 1423
Pérez-Torres, M. A., Romero-Cañizales, C., Alberdi, A., & Polatidis, A. 2009, A&A, 507, L17
Polatidis, A. G., & Aalto, S. 2000, in EVN Symp. 2000, Proc. the 5th european VLBI Network Symp., ed. J. E. Conway, A. G. Polatidis, R. S. Booth, & Y. M. Pihlström, 127
Polatidis, A. G., & Aalto, S. 2001, in IAU Symp., ed. R. T. Schilizzi, 198

Pounds, K. A., Reeves, J. N., King, A. R., & Page, K. L. 2004, MNRAS, 350, 10
Read, A. M. 2005, MNRAS, 359, 455
Sanders, D. B., Mazzarella, J. M., Kim, D., Surace, J. A., & Soifer, B. T. 2003, AJ, 126, 1607
Sargent, A., & Scoville, N. 1991, ApJ, 366, L1
Schulz, A., Henkel, C., Muders, D., et al. 2007, A&A, 466, 467
Schurch, N. J., & Warwick, R. S. 2002, MNRAS, 334, 811
Sergeev, S. G., Pronik, V. I., & Sergeeva, E. A. 2001, ApJ, 554, 245
Stevens, I. R., Read, A. M., & Bravo-Guerrero, J. 2003, MNRAS, 343, L47
Strickland, D. K., Heckman, T. M., Colbert, E. J. M., Hoopes, C. G., & Weaver, K. A. 2004, ApJS, 151, 193
Surcis, G., Tarchi, A., Henkel, C., et al. 2009, A&A, 502, 529
Takano, M., Mitsuda, K., Fukazawa, Y., & Nagase, F. 1994, ApJ, 436, L47
Tarchi, A., Henkel, C., Peck, A. B., & Menten, K. M. 2002a, A&A, 389, L39
Tarchi, A., Henkel, C., Peck, A. B., & Menten, K. M. 2002b, A&A, 385, 1049
Tarchi, A., Brunthaler, A., Henkel, C., et al. 2007a, A&A
Tarchi, A., Castangia, P., Henkel, C., & Menten, K. M. 2007b, New Astron. Rev.
Telesco, C. M., Decher, R., & Gatley, I. 1985, ApJ, 299, 896
Terashima, Y., Ptak, A., Fujimoto, R., et al. 1998, ApJ, 496, 210
Ulvestad, J. S. 2009, AJ, 138, 1529
Ulvestad, J. S., Wong, D. S., Taylor, G. B., Gallimore, J. F., & Mundell, C. G. 2005, AJ, 130, 936
Wang, Q. D., Chaves, T., & Irwin, J. A. 2003a, ApJ, 598, 969
Wang, Q. D., Chaves, T., & Irwin, J. A. 2003b, ApJ, 598, 969
Weaver, K. A., Heckman, T. M., Strickland, D. K., & Dahlem, M. 2002, ApJ, 576, L19
Wilson, A. S., & Ulvestad, J. S. 1982, ApJ, 263, 576
Zezas, A., Fabbiano, G., Rots, A. H., & Murray, S. S. 2002, ApJ, 577, 710
Zezas, A., Ward, M. J., & Murray, S. S. 2003, ApJ, 594, L31
Zhang, J. S., Henkel, C., Kadler, M., et al. 2006, A&A, 450, 933

Table 5. All galaxies known so far to host either H$_2$O(standard font) or OH (italics) maser emission, or both (bold face).

IRAS name	Alt. name	RA	Dec	Distance (Mpc)	$\log(L_{H_2O}^{iso})^a$ ($L_\odot$)	$\log(L_{OH}^{iso})^a$ ($L_\odot$)	Ref.[b]
00057+4021		00:08:20.5	+40:37:57	13 389	–	*1.93*	–, h10
00073+2538	NGC 23	00:09:53.6	+25:55:23	4566	2.2	*<–1.0*	w2, h11
00175+5902	IC 10	00:20:17.3	+59:18:14	–348	–0.74	<–3.6	w1, h2
N/A	NGC 235A	00:42:52.8	–23:32:28	6664	2.0	–	w3, –
00450–2533	**NGC 253**	00:47:33.1	–25:17:18	243	–0.74	–2.0	w1, h6
00461+3141	Mrk348	00:48:47.1	+31:57:25	4507	2.6	<–0.67	w1, h11
01063–8034	ESO013-G012	01:07:02.2	–80:18:28	5047	2.7	–	w1, –
01133+3249	Mrk1	01:16:07.2	+33:05:22	4780	1.7	–	w1, –
01219+0331	NGC 520	01:24:35.1	+03:47:33	2281	0.0	<–1.5	w5, h11
01310+3024	M33	01:33:50.9	+30:39:36	–179	–0.46	<–4.8	w1, h4
01306+3524	NGC 591	01:33:31.2	+35:40:06	4547	1.4	–	w1, –
01319–2940	NGC 613	01:34:18.2	–29:25:07	1481	1.2–1.5	–	w3–w5, –
01364–1042		01:38:52.9	–10:27:11	14 464	<0.56	*1.60*	w7, h10
01418+1651	*III Zw35*	01:44:30.5	+17:06:05	8225	<1.38	*2.39*	w3, h10
01562+2527		01:59:02.6	+25:42:37	49 665	–	*2.99*	–, h10
01573–0704	IC 0184	01:59:51.2	–06:50:25	5382	1.4	–	w3, –
02386–0828	NGC 1052	02:41:04.8	–08:15:21	1510	2.1	<0.31	w1, h1
02401–0013	**NGC 1068**	02:42:40.7	–00:00:48	1137	2.2	–0.08	w1, h5
02474+4127	NGC 1106	02:50:40.5	+41:40:17	4337	0.90	–	w2, –
02524+2046		02:55:17.1	+20:58:43	54 383	–	*3.35*	–, h10
02568+3637	Mrk1066	02:59:58.6	+36:49:14	3605	1.5	<0.20	w1, h3
03260–1422		03:28:24.3	–14:12:07	12 736	–	*2.04*	–, h10
03348–3609	NGC 1386	03:36:46.4	–36:00:02	868	2.1	–	w1, –
03355+0104	IRAS 03355+0104	03:38:10.4	+01:14:18	11 926	2.6	–	w7, –
03419+6756	IC 342	03:46:48.5	+68:05:46	31	–2	<–2.9	w1, h3
03521+0028		03:54:42.2	+00:37:03	45 541	–	*1.95*	–, h10
03566+1647		03:59:29.1	+16:56:26	40 029	–	*1.61*	–, h10
N/A	J0414+0534	04:14:37.8	+05:34:42	z = 2.64	4	–	w6, –
04121+0223		04:14:47.1	+02:30:36	36 702	–	*2.29*	, h10
04332+0209	*UGC3097*	04:35:48.4	+02:15:29	3590	–	*0.53*	–, h10
04454–4838	*ESO 203-IG-001*	04:46:49.5	–48:33:33	15 862	–	*2.51*	–, h10
04502+0258	UGC 3193	04:52:52.7	+03:03:24	4454	2.4	–	w2, –
05071+0725	UGC 3255	05:09:50.2	+07:29:00	5669	1.2	–	w1, –
05100–2425		05:12:09.2	–24:21:56	10 047	–	*1.35*	–, h10
06097+7103	Mrk3	06:15:36.3	+71:02:15	4050	1.0	<0.47	w1, h3
06106+7822	NGC 2146	06:18:37.7	+78:21:25	893	0.3	<–1.5	w1, h2
06206–3646		06:22:22.4	–36:47:43	32 390	–	*2.32*	–, h10
06256+6342	VIIZw073	06:30:25.6	+63:40:41	12 391	2.2	–	w3, –
06456+6054	NGC 2273	06:50:08.7	+60:50:45	1840	0.8	<–0.82	w4, h2
06487+2208		06:51:45.8	+22:04:27	42 972	–	*2.90*	–, h10
07163+0817		07:19:05.5	+08:12:07	33 269	–	*1.47*	–, h10
07151+5926	UGC 3789	07:19:30.9	+59:21:18	3325	2.6	–	w2, –
07379+6517	Mrk78	07:42:41.7	+65:10:37	11 137	1.5	–	w1, –
07572+0533		07:59:57.2	+05:25:00	56 900	–	*2.63*	–, h10
08014+0515	Mrk1210	08:04:05.8	+05:06:50	4046	1.9	–	w1, –
N/A	SDSSJ0804+3607	08:04:31.0	+36:07:18	z = 0.66	4.36	–	w8, –
08071+0509		08:09:47.2	+05:01:09	15 650	–	*1.90*	–, h10
08201+2801		08:23:12.6	+27:51:40	50 314	–	*3.30*	–, h10
08279+0956		08:30:40.9	+09:46:28	62 547	–	*2.98*	–, h10
08341–2614	He 2-10	08:36:15.2	–26:24:34	873	0.68	–	w9, –
N/A	2MASXJ0836+3327	08:36:22.8	+33:27:39	14 810	3.5	–	w7, –
08400+5023	NGC 2639	08:43:38.1	+50:12:20	3336	1.4	<–0.50	w1, h2
08449+2332		08:47:50.2	+23:21:10	45 406	–	*2.12*	–, h10
08474+1813		08:50:18.3	+18:02:01	43 591	–	*2.66*	–, h10
09039+0503		09:06:34.2	+04:51:25	37 516	–	*2.63*	–, h10
09108+4019	NGC 2782	09:14:05.1	+40:06:49	2543	1.1	<–0.65	w1, h2
09160+2628	NGC 2824	09:19:02.2	+26:16:12	2760	2.7	–	w1, –
09277+4917	SBS0927+493	09:31:06.7	+49:04:47	10 167	2.4	–	w7, –
09320+6134	**UGC 5101 (?; see text)**	09 35 51 6	+61 21 11	11 802	3.2	1.73	w4, h10
09380+0348	Mrk1419	09:40:36.4	+03:34:37	4932	2.6	–	w1, –
09407–1009	NGC 2979	09:43:08.6	–10:23:00	2720	2.1	–	w1, –
09430–1808	NGC 2989	09:45:25.8	–18:22:36	4146	1.6	–	w2, –
09531+1430		09:55:51.1	+14:16:01	64 538	–	*3.01*	–, h10
09517+6954	**NGC 3034–M 82**	09:55:52.7	+69:40:46	203	0.0	–2.1	w1, h6
09539+0857		09:56:34.3	+08:43:06	38 643	–	*3.26*	–, h10

Table 5. continued.

IRAS name	Alt. name	RA	Dec	Distance (Mpc)	$\log(L_{\mathrm{H_2O}}^{\mathrm{iso}})^a$ ($L_\odot$)	$\log(L_{\mathrm{OH}}^{\mathrm{iso}})^a$ ($L_\odot$)	Ref.^{b}
09585+5555	**NGC 3079**	10:01:57.8	+55:40:47	1116	2.7	−1.1	w1, h8
10039–3338	*IC 2545-ESO374-IG-032*	10:06:04.8	−33:53:15	10 223	<1.88	2.86	w14, h10
10036+2740		10:06:26.3	+27:25:46	49 466	–	1.99	–, h10
10140–3318	IC 2560	10:16:18.7	−33:33:50	2925	2.0	–	w1, –
10173+0828		10:20:00.2	+08:13:34	14 716	–	2.46	–, h10
10257–4338	NGC 3256	10:27:51.3	−43:54:14	2804	1.04	<0.65	w10, h7
10309+6017	Mrk34	10:34:08.6	+60:01:52	15 140	3.0	–	w1,–
10339+1548		10:36:37.9	+15:32:42	59 130	–	2.34	–, h10
10378+1109		10:40:29.2	+10:53:18	40 854	–	3.20	–, h10
10433+6329	NGC 3359	10:46:36.8	+63:13:25	1014	−0.15	<−1.5	w2, h2
10459–2453	NGC 3393	10:48:23.4	−25:09:43	3750	2.4–2.6	–	w3–w4, –
11010+4107	*Arp148*	11:03:53.2	+40:50:57	10 350	–	1.74	–, h10
11029+3130		11:05:37.5	+31:14:32	59 540	–	2.53	–, h10
11085+5556	NGC 3556	11:11:31.0	+55:40:27	699	0.0	<−1.7	w1, h2
11143–7556	NGC 3620	11:16:04.7	−76:12:59	1680	0.32	<0.04	w10, h7
11180+1623		11:20:41.7	+16:06:57	49 766	–	2.17	–, h10
11257+5850	**Arp299**	11:28:31.9	+58:33:45	3088	2.1	1.1	w1, h3
11330+7048	NGC 3735	11:35:57.3	+70:32:09	2696	1.1	<−0.50	w17, h2
11506–3851	*ESO320-G-030*	11:53:11.7	−39:07:49	3232	<1.66	1.52	w15, h10
11593–1835	Antennae	12:01:53.3	−18:52:37	1705	8.2	<−0.51	w9, h2
11524+1058		11:55:02.8	+10:41:44	53 564	–	2.81	–, h10
12005+0009		12:03:04.4	−00:07:27	36 646	–	2.02	–, h10
12005+4448	NGC 4051	12:03:09.6	+44:31:53	700	0.3	<−1.5	w1, h6
12018+1941		12:04:24.5	+19:25:10	50 559	–	2.49	–, h10
12032+1707		12:05:47.7	+16:51:08	65 291	–	4.15	–, h10
12080+3940	NGC 4151	12:10:32.6	+39:24:21	995	−0.2	<−1.4	w1, h2
12112+0305		12:13:46.0	+02:48:38	21 980	<1.89	2.78	w13, h10
12131+3636	NGC 4214	12:15:39.2	+36:19:37	291	0.028	<−2.6	w9, h2
12162+1047		12:18:47.7	+10:31:11	43 920	–	2.05	–, h10
N/A	NGC 4258	12:18:57.5	+47:18:14	448	1.9	<−2.1	w1, h2
12186+1839	NGC 4293	12:21:12.9	+18:22:57	893	0.1–0.7	<−2.1	w3, h4
12232+1256	NGC 4388	12:25:46.7	+12:39:44	2524	1.1	<−1.3	w1, h11
12243–0036	*NGC 4355*	12:26:54.6	−00:52:39	2179	<−0.14	−0.01	w5, h10
12315+0255	*NGC 4527*	12:34:08.5	+02:39:14	1736	0.60	–	w2, –
12540+5708	*Mrk231 - UGC 8058*	12:56:14.2	+56:52:25	12 642	<1.18	2.84	w4, h10
N/A	ESO 269-G012	12:56:40.5	−46:55:34	5014	3.0	–	w1, –
12548+2403		12:57:20.0	+23:47:46	39 483	–	1.89	–, h10
12590+2934	NGC 4922	13:01:25.2	+29:18:50	7071	2.3	<−0.47	w1, h11
13025–4911	NGC 4945	13:05:27.5	−49:28:06	563	1.7	<−1.5	w1, surcis
13218+0552		13:24:19.9	+05:37:05	61 488	–	3.07	–, h10
13277+4727	NGC 5194 (M51)	13:29:52.7	+47:11:43	463	−0.2	<−2.0	w1, h2
13362+4831	NGC 5256	13:38:17.2	+48:16:32	8353	1.5	<0.27	w1, h2
13370–3123	NGC 5253	13:39:55.9	−31:38:24	407	0.021	–	w9, –
13428+5608	*Mrk273-UGC 8696*	13:44:42.1	+55:53:13	11 326	<0.37	2.55	w16, h10
13451+1232	*4C +12.50*	13:47:33.3	+12:17:24	36 497	<2.25	2.28	w13, h10
13510+3344	NGC 5347	13:53:17.8	+33:29:27	2335	1.5	–	w1, –
14043+0624		14:06:49.8	+06:10:36	33 933	–	1.68	–, h10
14059+2000		14:08:18.7	+19:46:23	37 084	–	2.97	–, h10
14070+0525		14:09:31.2	+05:11:31	79 259	–	3.88	–, h10
14095–2652	NGC 5495	14:12:23.3	−27:06:29	6737	2.3	–	w3, –
14092–6506	Circinus	14:13:09.3	−65:20:21	434	1.3	–	w1, –
14106–0258	NGC 5506	14:13:14.8	−03:12:27	1853	1.7	<−0.47	w1, h2
14294–4357	NGC 5643	14:32:40.8	−44:10:29	1199	1.4	–	w1, –
14396–1702	NGC 5728	14:42:23.9	−17:15:11	2804	1.9	<−0.33	w1, h2
14547+2448	UGC 9618B	14:57:00.7	+24:37:03	10 094	2.8	–	w7, –
14553+1245		14:57:43.4	+12:33:16	37 444	–	1.94	–, h10
14566–1629	NGC 5793	14:59:24.7	−16:41:36	3491	2.0	–	w1, –
14586+1431		15:01:00.4	+14:20:15	44 279	–	2.54	–, h10
15065–1107	*NGC 5861*	15:09:16.1	−11:19:18	1851	–	0.04	–, h10
15107+0724	*CGCG049-057*	15:13:13.1	+07:13:32	3897	<0.43	0.85	w13, h10
15179+3956		15:19:47.1	+39:45:38	14 261	–	1.02	–, h10
15224+1033		15:24:51.5	+10:22:45	40 187	–	2.22	–, h10
15247–0945		15:27:27.8	-09:55:41	11 993	–	1.59	–, h10
15250+3609		15:26:59.4	+35:58:38	16 535	–	2.52	–, h10
15327+2340	*Arp220*	15:34:57.1	+23:30:11	5434	<−0.27	2.54	w16, h10
15587+1609		16:01:03.6	+16:01:03	41 126	–	3.04	–, h10

Table 5. continued.

IRAS name	Alt. name	RA	Dec	Distance (Mpc)	$\log(L_{H_2O}^{iso})^a$ $(L_\odot)$	$\log(L_{OH}^{iso})^a$ $(L_\odot)$	Ref.[b]
16100+2528		16:12:05.4	+25:20:23	39 688	–	1.68	–, h10
16255+2801		16:27:38.1	+27:54:52	40 056	–	2.38	–, h10
16300+1558		16:32:21.4	+15:51:46	72 467	–	2.71	–, h10
16399–0937		16:42:40.2	–09:43:14	8098	–	1.68	–, h10
16504+0228	NGC 6240	16:52:58.9	+02:24:03	7339	1.6	<–0.50	w1, h11
16552+2755	NGC 6264	16:57:16.1	+27:50:59	10 177	2.5	–	w7, –
17118+4350	NGC 6323	17:13:18.0	+43:46:56	7772	2.7	–	w1, –
17123–6245	NGC 6300	17:16:59.5	–62:49:14	1109	0.5	–	w1, –
17160+2006		17:18:15.6	+20:02:58	32 917	–	2.04	–, h10
17208–0014		17:23:21.9	–00:17:01	12 834	–	3.04	–, h10
17526+3253	*UGC 11035*	17:54:29.4	+32:53:14	7798	–	0.81	–, h10
17540+2935		17:55:56.1	+29:35:26	32 410	–	1.56	–, h10
18333–6528	ESO103-G35	18:38:20.3	–65:25:42	3983	2.6	–	w1, –
18368+3549		18:38:35.4	+35:52:20	34 827	–	2.81	–, h10
18544–3718		18:57:52.7	–37:14:38	22 012	–	2.23	–, h10
18588+3517		19:00:41.2	+35:21:27	31 996	–	2.12	–, h10
19370–0131	IRAS F19370-0131	19:39:38.9	-01:24:33	6622	2.2	–	w1, –
19497+0222	3C 403	19:52:15.8	+02:30:24	17 688	3.3	–	w1, –
20100–4156		20:13:29.5	–41:47:35	38 848	<4.44	3.77	w15, h10
20248+1734		20:27:08.9	+17:44:20	36 513	–	2.23	–, h10
20286+1846		20:30:55.5	+18:56:46	40 700	–	3.19	–, h10
20305–0211	NGC 6926	20:33:06.1	–02:01:39	5880	2.7	–	w1, –
20450+2140		20:47:14.3	+21:51:12	38 489	–	2.12	–, h10
20550+1656	*II Zw96*	20:57:23.9	+17:07:39	10 822	–	1.92	–, h10
21077+3358		21:09:49.0	+34:10:20	52 973	–	2.94	–, h10
21272+2514		21:29:29.4	+25:27:50	45 208	–	3.36	–, h10
21583–3800	AM2158-380b	22:01:17.1	–37:46:24	9983	2.7	–	w3, –
22025+4205	*UGC 11898*	22:04:36.1	+42:19:38	4290	–	0.86	–, h10
22055+3024		22:07:49.7	+30:39:40	38 041	–	2.36	–, h10
22088–1832		22:11:33.8	–18:17:06	51 026	–	2.59	–, h10
22116+0437		22:14:09.9	+04:52:24	58 098	–	2.26	–, h10
22265–1826	IRAS F22265-1826	22:29:12.5	–18:10:47	7520	3.8	–	w1, –
22491–1808		22:51:49.2	–17:52:23	23 312	–	1.82	–, h10
23019+3405		23:04:21.2	+34:21:48	32 389	–	1.78	–, h10
23024+1203	NGC 7479	23:04:56.7	+12:19:22	2381	1.3	<-1.3	w2, h6
23028+0725		23:05:20.4	+07:41:44	44 784	–	3.00	–, h10
23129+2548		23:15:21.4	+26:04:32	53 637	–	3.10	–, h10
23135+2516	*IC 5298*	23:16:00.7	+25:33:24	8221	<1.11	0.80	w3, h10
23168+0537	IC 1481	23:19:25.1	+05:54:22	6118	2.5	–	w1, –
23199+0122		23:22:31.6	+01:39:28	40 679	–	2.05	–, h10
23233+0946		23:25:56.2	+10:02:49	38 356	–	2.55	–, h10
23365+3604		23:39:01.3	+36:21:09	19 331	–	2.30	–, h10

Notes. [a] The lack of information on the maser luminosity (OH or H_2O), indicated by dashes, means that, to the best of our knowledge, neither a detection nor an upper limit for that transition was reported in the literature. [b] References: (w1) Henkel et al. (2005), A&A, 436, 75; (w2) Braatz & Gugliucci (2008), ApJ, 678, 96; (w3) Kondratko et al. (2006), ApJ, 638, 100; (w4) Zhang et al. (2006), A&A, 450, 933; (w5) Castangia et al. (2008), A&A, 479, 111; (w6) Impellizzeri et al. (2008), Nature, 456, 927; (w7) Kondratko et al. (2006), ApJ, 652, 136 (luminosities are derived directly from the spectra); (w8) Barvainis & Antonucci (2005), ApJ, 628, 89; (w9) Darling et al. (2008), ApJ, 685, 39; (w10) Surcis et al. (2009), A&A, 502, 529; (w11) Claussen et al. (1984), Nature, 310, 298; (w12) Hagiwara et al. (2002), A&A, 383, 65; (w13) Hagiwara et al. (2003), MNRAS, 344, 53; (w14) Greenhill et al. (2002), ApJ, 565, 836; (w15) Braatz et al. (1996), ApJS, 106, 51; (w16) Braatz et al. (2004), ApJ, 617, 29; (w17) Greenhill et al. (1997), ApJ, 486, 15; (h1) Norris et al. (1989), MNRAS, 237, 673; (h2) Baan et al. (1992), AJ, 103, 728; (h3) Staveley-Smith et al. (1987), MNRAS, 226, 689; (h4) Schmelz & Baan (1988), AJ, 95, 672; (h5) Gallimore et al. (1996), ApJ, 462, 740; (h6) Unger et al. (1986), MNRAS, 220, 1; (h7) Staveley-Smith et al. (1992), MNRAS, 258, 725; (h8) Baan & Irwin (1995), ApJ, 446, 602; (h9) Baan et al. (1982), ApJ, 260, 49; (h10) Klöckner (2004), Ph.D. Thesis, and references therein; (h11) Schmelz et al. (1986), AJ, 92, 1291.